JOURNAL OF PETROLOGY | VOLUME 47 | NUMBER 10 | PAGES 1915–1942 | 2006 | doi:10.1093/petrology/egl031

Syros Metasomatic Tourmaline: Evidence for Very High-δ^{11}B Fluids in Subduction Zones

HORST R. MARSCHALL[1]*, THOMAS LUDWIG[1], RAINER ALTHERR[1], ANGELIKA KALT[2] AND SONIA TONARINI[3]

[1]MINERALOGISCHES INSTITUT, UNIVERSITÄT HEIDELBERG, IM NEUENHEIMER FELD 236, D-69120 HEIDELBERG, GERMANY

[2]INSTITUT DE GÉOLOGIE, UNIVERSITÉ DE NEUCHÂTEL, RUE EMILE ARGAND 11, CH-2007 NEUCHÂTEL, SWITZERLAND

[3]ISTITUTO DI GEOSCIENZE E GEORISORSE, CNR, VIA MORUZZI 1, I-56124 PISA, ITALY

RECEIVED SEPTEMBER 19, 2005; ACCEPTED MAY 8, 2006; ADVANCE ACCESS PUBICATION JUNE 6, 2006

High-pressure (HP) metamorphic blocks enclosed in a mafic to ultramafic matrix from a mélange on the island of Syros are rimmed by tourmaline-bearing reaction zones (blackwalls). The B isotopic composition of dravitic tourmaline within these blackwalls was investigated in situ by secondary ion mass spectrometry. Boron in these tourmalines is unusually heavy, with $\delta^{11}B$ values exceeding +18‰ in all investigated samples and reaching an extreme value of +28·4‰ in one sample. Blackwalls formed during exhumation of the HP mélange at a depth of 20–25 km at temperatures of 400–430°C, by influx of external hydrous fluids. The compositions of the fluids are estimated to be in the range of 100–300 μg/g B with $\delta^{11}B$ values of +18 to +28‰. The high $\delta^{11}B$ values cannot be explained by tourmaline formation from unmodified slab-derived fluids. However, such fluids could interact with the material in the exhumation channel on their way from the dehydrating slab to the site of tourmaline formation in the blackwalls. This could produce exceptionally high $\delta^{11}B$ values in the fluids, a case that is modelled in this study. The model demonstrates that subduction fluids may be effectively modified in both trace element and isotopic composition during their migration through the material overlying the subducting slab. Blackwall tourmaline from Syros has a large grain size (several centimetres), high abundance, and an exceptionally high $\delta^{11}B$ value. The formation of tourmaline at the contact between mafic or felsic HP blocks and their ultramafic matrix involved fluids released during dehydration reactions in the subducting slab. It forms a heavy-boron reservoir in hybrid rocks overlying the subducting slab, and may, thus, have a significant impact on the geochemical cycle of B and its isotopes in subduction zones.

KEY WORDS: *boron isotopes; tourmaline; subduction zone; fluid, high pressure*

INTRODUCTION

Important constraints on the mechanisms of slab-to-mantle material transfer can be derived from the abundance and isotopic systematics of boron in subduction-related rocks. Element ratios such as B/Be and B/Nb and B isotope signatures have been used over the last ~20 years to enhance our knowledge of slab dehydration and subduction-related melting processes. The high relative mass difference of the two stable isotopes of boron (^{10}B and ^{11}B) is responsible for variations in its isotopic composition in nature of about 100‰ (Palmer & Swihart, 2002). The large B isotopic fractionation at low temperatures has led to the use of the B stable isotope system for studies of processes acting at the Earth's surface (e.g. Hemming & Hanson, 1992; Barth, 1998) and for the detection of chemical and isotopic signals of subducted material in fluids, serpentinites and subduction-related volcanic rocks (e.g. Ishikawa & Nakamura, 1994; Benton *et al.*, 2001). B is known to be relatively mobile in hydrous fluids and in silicate melts (e.g. Brenan *et al.*, 1998*a*, 1998*b*). B concentrations in the slab decrease with increasing depth of subduction, as it is released with fluids during dehydration (Moran *et al.*, 1992; Bebout *et al.*, 1999). Concurrently, preferential loss of the heavier isotope ^{11}B

*Corresponding author. Present address: Department of Earth Sciences, University of Bristol, Wills Memorial Building, Queen's Road, Bristol BS8 1RJ, UK. Telephone: +44-117-3315006. Fax: +44-117-9253385. E-mail: Horst.Marschall@bristol.ac.uk

results in decreasing $\delta^{11}B$ values in the subducting material (Peacock & Hervig, 1999). Studies on subduction-related volcanic rocks investigating across-arc transects show a decrease of B concentrations, B/Be and B/Nb ratios and $\delta^{11}B$ values from trench to back-arc (Ishikawa & Nakamura, 1994; Ishikawa & Tera, 1997; Benton *et al.*, 2001; Ishikawa *et al.*, 2001). Within the slab, the most important reservoirs for B are sediments, altered magmatic rocks and serpentinized ultramafic rocks (e.g. Leeman & Sisson, 2002; Scambelluri *et al.*, 2004). Fresh mantle and magmatic rocks have very low B concentrations and a relatively uniform B isotope ratio. Sediments, altered magmatic rocks and serpentinites are not only enriched in B, but also show $\delta^{11}B$ values higher than mid-ocean ridge basalt (MORB) (or mantle), as a result of the interaction with seawater, which has a very high $\delta^{11}B$ value. The hydrous portion of the subducting slab, therefore, introduces large amounts of heavy B into the subduction zone.

Tourmaline

Tourmaline is the most widespread borosilicate mineral in natural rocks. It contains ~3 wt % B, an element that is of very low abundance in most crustal and mantle rocks (e.g. Ryan & Langmuir, 1993; Chaussidon & Jambon, 1994; McDonough & Sun, 1995; Taylor & McLennan, 1995). Therefore, formation of tourmaline requires effective concentration of B, even if it is formed in rocks of the continental crust. This concentration is attained either (1) by magmatic differentiation, forming tourmaline in pegmatites enriched in B as a result of its highly incompatible character, or (2) by fluid-dominated processes because of the highly fluid-mobile character of B. The B necessary for tourmaline growth in fluid-saturated rocks may be supplied by other phases within the rock itself, such as clay minerals or mica (Nakano & Nakamura, 2001) or by external fluids during metasomatism (Altherr *et al.*, 2004). Once formed, tourmaline is highly stable in a large variety of rock types over an exceptionally large P–T range, including conditions in subducting slabs to depths of ~250 km (Werding & Schreyer, 2002).

Tourmaline from (ultra-)HP metamorphic rocks has been used to unravel the evolution of the B isotopic composition of rocks composing the subducted slab. It has been demonstrated by Bebout & Nakamura (2003) that the $\delta^{11}B$ values of tourmaline decrease during prograde growth, are very low in HP growth zones, and increase in retrograde growth zones. Intracrystalline isotopic equilibration by diffusion is very limited and different growth zones still display their initial isotopic compositions. Tourmaline, therefore, provides a powerful tool to monitor the B isotope evolution of metamorphic rocks and provides important insights into the B isotope budget of metamorphic fluids.

Boron isotope ratios of tourmaline from metasomatic reaction zones in HP metamorphic rocks from the island of Syros are presented in this paper. Implications for $\delta^{11}B$ values of subduction zone fluids, together with a model providing an explanation for the extremely heavy B isotopic composition of Syros tourmaline, will be discussed.

ANALYTICAL METHODS

Compositions of mineral phases were determined using a Cameca SX 51 electron microprobe equipped with five wavelength-dispersive spectrometers (Mineralogisches Institut, Heidelberg). Operating conditions were 20 nA beam current and 15 kV acceleration voltage. For analyses of phengite, the electron beam was defocused to 10 μm to avoid loss of alkalis. For analyses of tourmaline it was defocused to 5 μm. Details on counting times, crystals, standards and detection limits have been given by Marschall (2005). PAP correction was applied to the raw data (Pouchou & Pichoir, 1984, 1985).

For tourmaline, a modified matrix correction was applied assuming stoichiometric oxygen and all non-measured components to be B_2O_3. The accuracy of the electron microprobe analyses of tourmaline and the correction procedure was checked by measuring three samples of reference tourmalines (98144, elbaite; 108796, dravite; 112566, schorl; Dyar *et al.*, 1998, 2001). Under the described conditions, analytical errors on all analyses are ±1% relative for major elements and ±5% relative for minor elements. A detailed description of the electron microprobe techniques for tourmaline analysis has been given by Kalt *et al.* (2001).

Concentrations of H, Li and B and B isotope ratios were measured by secondary ion mass spectrometry (SIMS) with a modified Cameca IMS 3f ion microprobe at the Mineralogisches Institut, Heidelberg, equipped with a primary beam mass filter. Secondary ions ^{7}Li and ^{11}B in tourmaline were collected under an ion-imaged field of 150 μm diameter (Kalt *et al.*, 2001). Secondary ions of ^{1}H were collected by reducing the 25 μm beam spot to an ion-imaged field of 12 μm by using a field aperture, to minimize the influence of surface contamination (Marschall & Ludwig, 2004). Water contamination was further reduced using a cold-trap cooled with liquid nitrogen attached to the sample chamber of the IMS 3f. The relative ion yields (RIY) for H and B were determined using three tourmalines as reference material: elbaite (98144), dravite (108796) and schorl (112566). The relative reproducibility (1σ) of the analyses of B was <1%. For Li the reference material

was NIST SRM 610 (Pearce *et al.*, 1997) with a relative reproducibility of <1%. The accuracy is limited by matrix effects and the uncertainty of the element concentrations in the reference material; the relative uncertainty is estimated to be <25% for H, <20% for Li and <10% for B (Kalt *et al.*, 2001). Between 10 and 20 Li and B analyses and 5–10 H analyses were performed on tourmaline in each sample.

The analysis of boron isotope ratios required significant changes of both software and hardware of the SIMS. Most important were changes in the electronic control device of the magnet, which permitted faster switches between different masses and better stability of the magnet. The changes have been described in detail by Marschall (2005).

The primary ion beam was $^{16}O^-$ accelerated to 10 keV with a beam current of 1 nA, resulting in count rates for ^{11}B of $\sim 2 \times 10^5$ s^{-1} and $\sim 5 \times 10^4$ s^{-1} for ^{10}B on tourmaline, collected by a single electron multiplier. The diameter of the 1 nA spot was $\leq 5\,\mu m$. The energy window was set to 50 eV and no offset was applied. Fifty cycles were measured on each analysis spot with counting times of 3·307 s and 1·660 s on ^{10}B and ^{11}B, respectively. Presputtering lasted for 5 min and the settling time between two different masses was 200 ms, resulting in total analysis time for one spot of ~10 min. The internal precision of a single analysis was ≤1‰ (2σ). Boron isotopic compositions of samples are reported using the δ-notation ($\delta^{11}B$ in ‰) relative to the SRM 951 accepted value (Catanzaro *et al.*, 1970). Instrumental mass fractionation was corrected for by using three samples of reference tourmaline (98114, elbaite; 108796, dravite; 112566, schorl; Leeman & Tonarini, 2001). Correction factors α_{inst} for the different reference tourmalines resulted in a mean α_{inst} of 1·0476. Reproducibility of measured isotope ratios during the analytical session (8 days) was ±0·5‰.

During analysis of tourmaline samples by SIMS, traverses through different grains were measured to check for possible intra-grain variations in $\delta^{11}B$. Between 10 and 50 boron isotope analyses were performed for each sample. SIMS analysis of our samples revealed very high $^{11}B/^{10}B$ ratios in contrast to the reference tourmalines, which range from –12·5‰ to –6·6‰ (Leeman & Tonarini, 2001). To ensure consistency, three tourmaline samples from Syros were analysed by positive thermal ion mass spectrometry (P-TIMS), following the method of Tonarini *et al.* (1997). Correlation between SIMS and P-TIMS results for three Syros samples and the three reference tourmalines demonstrate good correlation between the two methods (see Fig. 2) used in the two laboratories. This proves the instrumental mass fractionation of SIMS to be independent of $^{11}B/^{10}B$ ratios in the range of $\delta^{11}B$ in natural tourmaline.

GEOLOGICAL BACKGROUND

The island of Syros displays a sequence of rocks belonging to the lower unit of the Attic–Cycladic Crystalline Complex (Dürr *et al.*, 1978). The major part of the island is composed of interlayered schists and marbles dipping north to NE (e.g. Hecht, 1984; Dixon & Ridley, 1987; Seck *et al.*, 1996). They were interpreted as metamorphosed flysch sediments by Dixon & Ridley (1987). The most interesting formations are exposed in the northern part of Syros near Kámpos and along the coastline around Hermoupolis and Kini (Fig. 1). These formations are composed of metagabbro, eclogite, glaucophane schist, meta-plagiogranite, serpentinite and metasediment, which all mainly preserve a blueschist- to eclogite-facies metamorphic overprint. The structural and tectono-metamorphic evolution of the island of Syros and especially its northern part has been investigated in a large number of studies (Dixon, 1968; Bonneau *et al.*, 1980; Ridley, 1982, 1984, 1986; Ballhaus & Schumacher, 1995; Trotet *et al.*, 2001*a*; Rosenbaum *et al.*, 2002; Ring *et al.*, 2003; Brady *et al.*, 2004; Keiter *et al.*, 2004). Most workers distinguish three ductile deformation phases along a single clockwise *P–T* path: (1) prograde deformation; (2) deformation near the peak pressure of metamorphism; (3) retrograde deformation. The prograde *P–T* path is characterized by a high *P/T* ratio, typical for subduction zone metamorphism. Peak metamorphic conditions have been estimated at ~470–520°C and 1·3–2·0 GPa by different workers for different rock types (Dixon, 1968; Ridley, 1984; Okrusch & Bröcker, 1990; Trotet *et al.*, 2001*b*; Rosenbaum *et al.*, 2002; Keiter *et al.*, 2004). The exhumation path of the rocks is characterized by near-isothermal decompression, resulting in the preservation of the HP assemblages and minerals. Trotet *et al.* (2001*b*) showed that the rocks from Syros were decompressed at temperatures between 400 and 550°C to pressures between 1·0 and 0·5 GPa. For a clinopyroxene + albite + glaucophane-bearing retrograde assemblage they calculated conditions of 0·78 GPa and 394°C. This is in line with the occurrence of fresh lawsonite in some places around the island (Dixon, 1968; Brady *et al.*, 2001; Marschall, 2005), because this mineral easily decomposes upon heating.

The above-mentioned units of metabasites occur in the upper level of the major marble–schist sequence. The internal structure of the northern mélange in the area of Kámpos (Fig. 1), which is the best investigated area, is rather complex. A number of rock types have been distinguished on the basis of geochemical and petrographic observations within an east–west-trending zone. They are interpreted as the high-pressure metamorphic equivalents of different parts of ancient oceanic crust (e.g. Seck *et al.*, 1996). West of Kámpos, the various rock types form a mélange with blocks of eclogite, omphacite/jadeite fels (the term fels in this

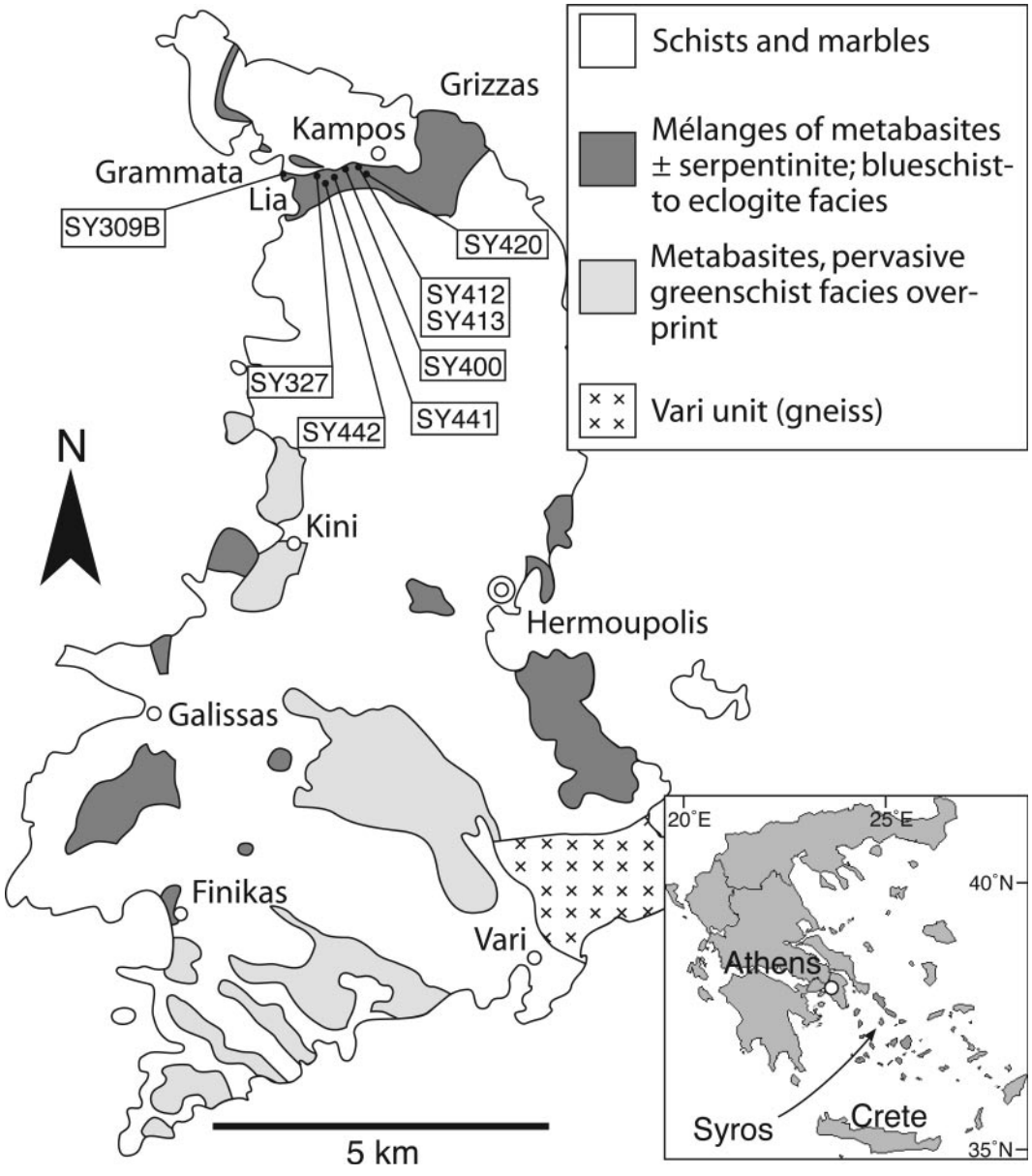

Fig. 1. Simplified geological map of Syros after Hecht (1984), showing sample localities within the mafic–ultramafic mélange near Kampos. Inset shows a map of Greece with the location of the island of Syros.

paper refers to a metamorphic rock with an isotropic fabric), garnet glaucophane fels, serpentinite and metagabbro embedded in a matrix of chlorite schist and serpentinite (Dixon, 1968; Hecht, 1984; Dixon & Ridley, 1987; Okrusch & Bröcker, 1990; Seck *et al.*, 1996; Bröcker & Enders, 2001). Contact between the blocks and their chemically and mineralogically contrasting matrix are characterized by reaction zones rich in OH-bearing minerals (Fig. 3a), which are referred to subsequently as 'blackwalls'. Blackwall rocks are hybrids as they have no pre-metamorphic equivalent of comparable chemical composition, but were formed from two different precursor rocks by tectonic mixing and/or metasomatic transfer of material. This process of blackwall formation on Syros was previously described by Dixon (1968) and other workers (Ridley, 1984; Dixon & Ridley, 1987; Okrusch & Bröcker, 1990; Ballhaus & Schumacher, 1995; Seck *et al.*, 1996; Bröcker & Enders, 2001), and is also known from other high-pressure terranes, such as Cima di Gagnone, Alps, Switzerland (Rice *et al.*, 1974; Evans *et al.*, 1979), Santa Catalina Island, California, USA (Sorensen & Grossman, 1989;

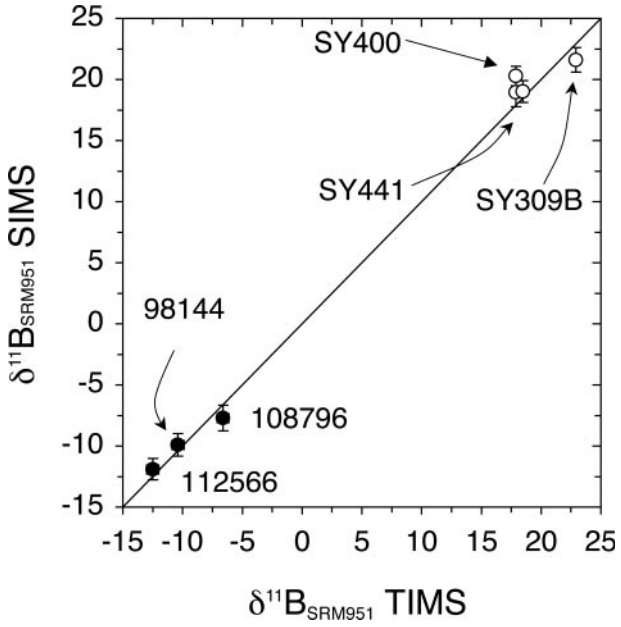

Fig. 2. Comparison of B isotope ratios of tourmaline determined by SIMS and TIMS, expressed in the δ-notation relative to NIST SRM 951 (Catanzaro *et al.*, 1970). ○, Syros samples; ●, standard tourmalines (Leeman & Tonarini, 2001). For sample SY400, core and rim values differ by ∼1·3‰, which is shown by the two data points. Error bars show 2σ errors of SIMS (∼1‰). Errors for TIMS (∼0·5‰) are within the size of the symbols.

Bebout & Barton, 2002), the Franciscan Complex, California, USA (King *et al.*, 2003), Port Macquarie, New South Wales, Australia (Och *et al.*, 2003) and NE New Caledonia (Carson *et al.*, 2000; Spandler *et al.*, 2003; Fitzherbert *et al.*, 2004).

INVESTIGATED SAMPLES

The eight blackwall samples investigated in this study (Table 1) were taken from different places within the mélange (Fig. 1). They all contain significant amounts of tourmaline, concentrated in millimetre- to centimetre-thick layers on the surface of the high-pressure blocks (Fig. 3b and c), or more evenly distributed single crystals or clusters of crystals (Fig. 3d) within them. Two samples (SY309B, SY420) are schists from the matrix, which contain tourmaline-rich layers or veins. Apart from tourmaline, the blackwall rocks contain omphacite ($Jd_{35–53}$), chlorite (clinochlore), phengite (3·3–3·4 Si per 11 oxygens), and almost pure albite ($Ab_{97–100}$). Some samples additionally contain biotite (Table 1). Quartz was not observed in any of the samples. Tourmaline in all samples is euhedral and does not show any sign of brittle or ductile deformation. In thin section, the grains commonly show visible zonation. Colours of the pleochroic cores change from colourless to blue, whereas those of the rims change from pale pink to green. Rims of tourmaline in some samples (SY400, SY441, SY442) show two or three zones with different shades of green. Resorption of core domains and replacement by rim material is limited, and resorption of rim domains was never observed.

Sample SY309 is composed of glaucophane schist (SY309A) and tourmaline-rich layers (SY309B). The latter are concordant with the foliation of the host rock and can be tracked over several metres in the outcrop. Sample SY309B, a 1–2 cm thick layer consisting of tourmaline + omphacite + chlorite + albite + phengite + glaucophane + epidote + apatite + rutile + titanite, is hosted in a glaucophane schist composed of glaucophane + epidote + phengite + titanite. Tourmaline crystals are 0·1–1·0 mm in diameter and 1–6 mm in length with some inclusions of titanite, rutile, omphacite, albite ($Ab_{99·7}$) and apatite.

Sample SY327 is a dark green omphacite–chlorite fels consisting of equal amounts of chlorite and omphacite, making up about 80% of the rock. Additional phases are abundant apatite (2–3 mm), albite, ilmenite, titanite, biotite, amphibole and tourmaline. Three compositional types of clinopyroxene were observed in the matrix. The first type forms the cores of large omphacite grains (1–5 mm) with intermediate acmite and jadeite contents ($Jd_{37}Acm_{28}Q_{34}$). The second type is found as rims of the same grains with a much higher jadeite content ($Jd_{52}Acm_{27}Q_{19}$). The third type is found in patches composed of small grains (10 μm) closely intergrown with albite (Ab_{97}). Type-3 clinopyroxene has high acmite and very low jadeite contents ($Jd_{15}Acm_{49}Q_{35}$ = aegirine). Garnet is not preserved in the rock, but was probably present before, as indicated by hexagonal pseudomorphs consisting of fine-grained chlorite. Amphibole occurs only as small inclusions (<100 μm) in tourmaline and is zoned from blue in the core to bluish green at the rim, with compositions changing from glaucophane to nyböite and magnesiokataphorite. Tourmaline grains are ∼4 mm in diameter and 3 cm in length and are highly poikiloblastic with inclusions of predominantly omphacite, blue–green amphibole, apatite and chlorite.

Sample SY400 is a pale green tourmaline–omphacite–chlorite fels (Fig. 3d), consisting primarily of chlorite and fine-grained omphacite with minor epidote, phengite and accessory rutile, titanite and apatite. Tourmaline crystals are 2–5 mm in diameter and 10–20 mm in length and highly poikiloblastic with inclusions of omphacite, rutile, titanite, apatite and epidote. The rock itself shows healed cracks (about 1 mm wide) filled by chlorite and prismatic omphacite, grown perpendicular to the cracks' elongation. The cracks can be traced pseudomorphically through the large tourmaline grains by zones of lower inclusion density. Tourmaline itself is

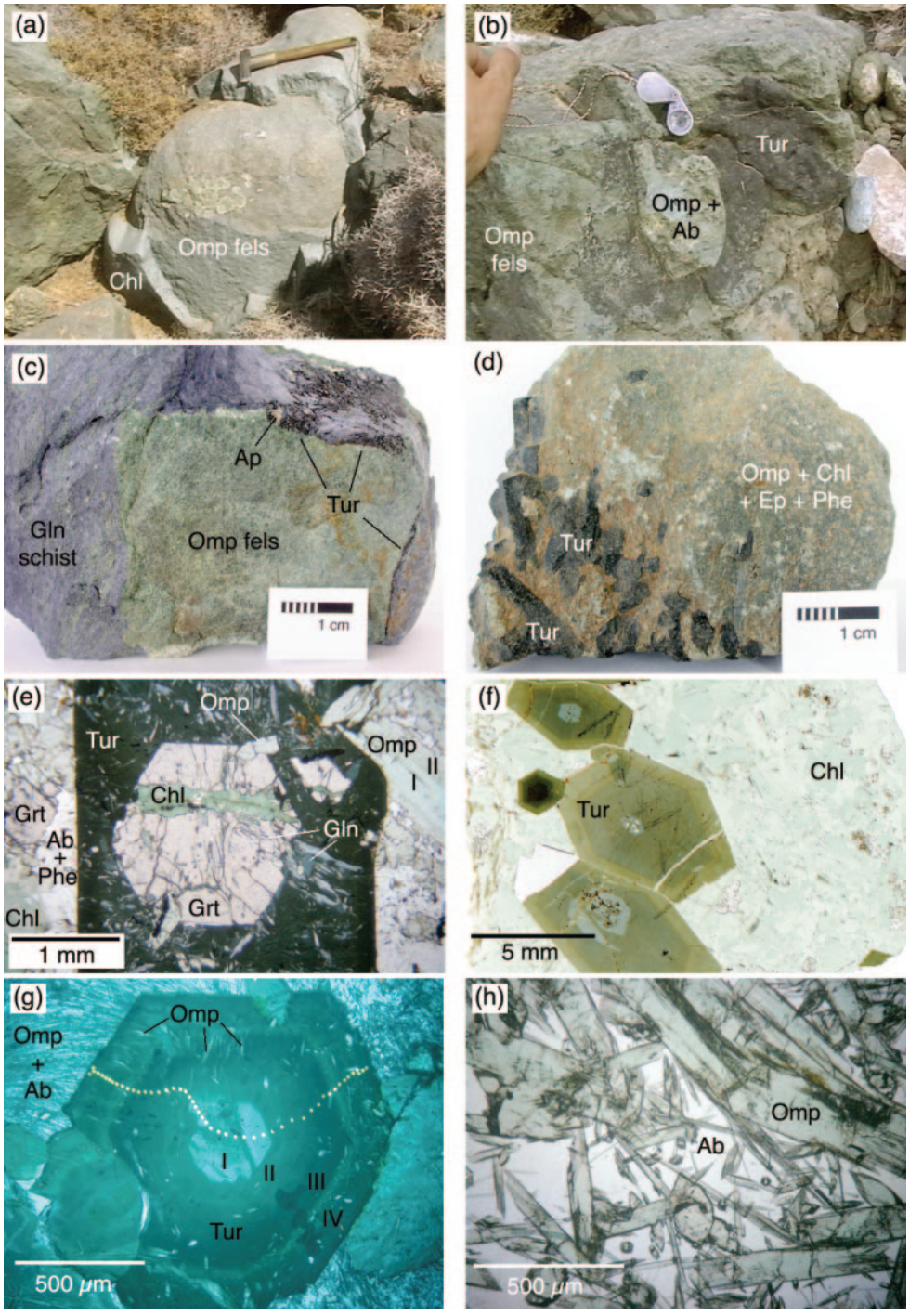

Fig. 3. Different varieties of blackwalls in the field, in hand specimen and in thin section. (a) Omphacite (Omp) fels enveloped by an ~10 cm thick layer of almost pure chlorite (Chl). (b) Tourmaline (Tur, black) covering an HP block in a dense layer. (c) Tourmaline and apatite (Ap) at the contact between an omphacite fels and the surrounding glaucophane schist. (d) Centimetre-sized tourmaline crystals in the outer zone of an omphacite fels. (e) Plane-polarized light photomicrograph of thin section of sample SY412, showing an idioblast of garnet (Grt), truncated by a chlorite-filled crack and enclosed in a large tourmaline crystal (dark). Omphacite (Omp) included in tourmaline also shows type-I cores partly replaced by type-II rims, similar to the omphacite in the matrix. (f) Photomicrograph of thin section of sample SY441, showing large zoned tourmaline crystals in paragenesis with chlorite (unpolarized light). (g) and (h) are photomicrographs of thin section of sample SY442. (g) Zoned tourmaline crystal with small omphacite inclusions. The thin section was covered with a gold layer prior to SIMS analysis, producing the dark blue colours of the picture. The spots generated during SIMS analyses are visible as white dots. I, II, III and IV refer to zones I–IV, respectively (see text and Fig. 7). (h) Detail of the matrix surrounding tourmaline in (g) consisting of euhedral and subhedral omphacite intergrown with albite.

Table 1: List of tourmaline-bearing blackwall and mélange matrix samples investigated for B isotope ratios

Sample	Rock type	Mineral assemblage	Tur diameter* (mm)
SY309B	Gln schist†	Tur, Chl, Omp, Gln, Phe, Ab, Czo, Ap, Ttn, Rt	0·1–0·5
SY327	Omp–Chl fels	Omp, Chl, Ab, Tur, Ap, Ttn, Ilm, Am, Bt	3–4
SY400	Omp–Chl fels	Omp, Chl, Phe, Tur, Czo, Rt, Ttn, Ap	2–5
SY412	Eclogite‡	Omp, Chl, Phe, Tur, Grt, Czo, Gln, Ab, Bt, Rt	1–3
SY413	Gln schist	Gln, Czo, Chl, Phe, Omp, Tur, Ab, Ttn	4–5
SY420	Phe–Ep–Grt schist	Tur, Chl, Phe, Czo, Grt, Ab, Ttn, Rt, Aln	0·1–0·5
SY441	Chl schist	Chl, Tur, Omp, Ttn, Rt, Aln	4–5
SY442	Omp–Ab fels	Omp, Ab, Tur, Ttn	0·5–1·5

Minerals are listed in order of decreasing abundance.
*Diameters of tourmaline are given for sections perpendicular to the *c*-axes.
†SY309B is a layer of Tur + Omp + Chl + Ab + Phe, formed within a glaucophane schist consisting of Gln + Czo + Phe + Ttn.
‡SY412 is a former eclogite the paragenesis of which is partly replaced by the assemblage Tur + Bt + Chl + Ab + Phe.

not deformed or cracked. Therefore, tourmaline growth obviously postdates both chloritization and deformation.

Sample SY412 was taken from an interior part of an eclogite block, which shows a transition into a glaucophane-rich assemblage at its margins (see SY413 below). The eclogitic paragenesis of SY412 is garnet + type-1 omphacite + rutile + phengite + glaucophane + epidote (± quartz?). This primary assemblage is partly replaced by a secondary assemblage of dominantly hydrous minerals, which form small, closely intergrown aggregates between the larger primary phases. The secondary assemblage is composed of phengite + glaucophane + albite + chlorite + type-2 omphacite + tourmaline. In some patches, biotite formed at the expense of phengite. The eclogitic garnet contains inclusions of glaucophane and is partly pseudomorphosed by chlorite. It shows chemical zonation with decreasing Mn content and increasing Fe and Mg contents from core to rim (Table 2). Omphacite is chemically zoned with type-1 cores ($Jd_{42}Acm_{15}Q_{41}$) and type-2 omphacite rims ($Jd_{53}Acm_{30}Q_{14}$). Rutile is still abundant and shows only thin overgrowths of titanite (<5 μm). Tourmaline forms large grains 1–3 mm in diameter and 5–15 mm in length, with inclusions of omphacite, glaucophane, garnet, phengite, epidote, albite and rutile (Fig. 3e). Garnet grains included in tourmaline show incipient chloritization along cracks, which was obviously stopped by the shielding tourmaline (Fig. 3e). Furthermore, tourmaline locally grew into the chlorite-filled cracks in garnet. Therefore, we conclude that tourmaline replaced chlorite, but did not interact with garnet. Garnet rims are in direct contact with tourmaline and type-2 omphacite. The observed petrographic relationship of the minerals (i.e. tourmaline, omphacite, chlorite and garnet) are very similar to those described by Altherr *et al.* (2004).

Sample SY413 is part of the glaucophane-rich envelope of the above-described block of sample SY412. The rock is dominated by glaucophane and chlorite pseudomorphs after garnet, accompanied by phengite, omphacite, albite, titanite, tourmaline and epidote. Long-prismatic omphacite grains occur throughout the rock and also inside the large, poikiloblastic tourmaline grains. Further inclusions in tourmaline are glaucophane, rutile, titanite, albite, chlorite and epidote. Tourmaline grains are about 5 mm in diameter and 20–30 mm in length. Omphacite is homogeneous ($Jd_{45}Acm_{12}Q_{43}$). The paragenesis glaucophane + chlorite + albite + omphacite + phengite + tourmaline, which is found in some places in the core of the eclogite block (represented by sample SY412) is the dominant mineral assemblage of sample SY413. Garnet is entirely transformed to chlorite, and rutile is replaced by titanite.

Sample SY420 is a schist from the matrix surrounding the blocks of the Syros mélange. The rock is foliated and folded and shows layering with alternating epidote- and chlorite-rich layers, both of which contain abundant tourmaline, phengite, garnet and albite. Accessories are allanite (in the core of epidote), rutile and titanite. Rutile forms large inclusions (500 μm) in garnet. Garnet has developed a chemical zonation with Mn-rich cores ($Alm_{57}Sps_7Grs_{28}Prp_4Adr_4$) and Fe-rich mantles ($Alm_{63}Sps_2Grs_{26}Prp_5Adr_4$). The mantle is partially resorbed and replaced by chlorite + albite. Some grains, however, show newly grown rims with Ca- and Mn-rich compositions ($Alm_{26}Sps_{34}Grs_{31}$-Prp_5Adr_4). They show a sharp contrast to the Fe-rich mantle without diffusional equilibration. Tourmaline grains are 0·1–0·5 mm in diameter and 1–3 mm in length. Inclusions in tourmaline are epidote and rutile.

Sample SY441 is part of a blackwall that consists almost exclusively of coarse-grained chlorite and clusters

Table 2: Representative electron microprobe analyses of different minerals

Mineral:	Omp						Gln			Phe			Grt		Chl			Ab			
Sample:	SY309B	SY412		SY413	SY442		SY309B	SY412	SY413	SY309B	SY412	SY413	SY412		SY309B	SY412	SY413	SY309B	SY412	SY413	SY442
Type:		I (core)	II (rim)		core	rim							core	rim							
SiO_2	55·46	55·67	56·25	55·80	55·21	56·03	57·89	56·48	56·87	53·05	51·28	52·17	37·49	37·84	27·67	25·33	27·34	69·44	69·74	69·33	69·51
TiO_2	0·08	0·20	0·06	0·16	0·08	0·05	0·02	0·05	0·04	0·05	0·25	0·10	0·20	0·08	0·02	0·02	0·00	0·04	0·02	0·01	
Al_2O_3	8·90	10·20	12·29	10·54	8·34	12·41	9·99	9·47	9·34	25·48	26·61	24·94	20·41	20·92	20·01	19·93	19·17	19·04	18·96	18·76	19·05
Cr_2O_3	0·15	0·00	0·02	0·07	0·00	0·01	0·11	0·02	0·04	0·13	0·03	0·10	0·02	0·01	0·14	0·02	0·06				0·02
Fe_2O_3	6·60	5·50	11·33	4·37	8·14	7·00	2·79	5·95	4·14				1·11	0·75				0·23	0·05	0·13	0·12
FeO	1·91	3·98	2·97	3·43	3·86	3·86	7·35	8·49	9·27	2·67	4·03	4·07	24·02	26·29	15·70	28·34	21·59				
MnO	0·15	0·00	0·06	0·13	0·16	0·08	0·11	0·18	0·11	0·01	0·00	0·08	5·19	4·22	0·28	0·75	0·44		0·01	0·01	0·06
MgO	7·31	6·17	1·97	6·33	6·00	3·64	11·56	9·28	9·21	4·05	3·00	3·50	1·40	1·73	22·91	13·04	19·09	0·01			
CaO	11·53	10·90	3·56	11·26	10·28	6·41	0·45	0·96	0·51	0·00	0·01	0·06	10·23	9·10	0·01	0·02	0·02		0·01	0·02	0·10
Na_2O	7·87	8·14	12·12	8·11	8·24	10·44	7·36	7·06	7·14	0·14	0·59	0·23	0·03	0·00	0·01	0·01	0·00	11·94	12·13	12·00	11·78
K_2O	0·01	0·01	0·01	0·00	0·00	0·00	0·01	0·14	0·02	10·59	10·41	10·44	0·00	0·00	0·00	0·04	0·03	0·04	0·03	0·03	0·05
H_2O							2·20	2·16	2·14	4·54	4·50	4·48			11·86	11·12	11·61				
Total	99·95	100·77	100·63	100·19	100·30	99·93	99·87	100·23	98·83	100·72	100·71	100·16	100·10	100·94	98·62	98·61	99·35	100·74	100·95	100·29	100·69
Si	1·993	1·989	2·007	1·995	1·998	2·005	7·936	7·846	7·971	3·504	3·417	3·492	2·995	2·996	2·798	2·733	2·823	3·011	3·018	3·021	3·015
Ti	0·002	0·005	0·002	0·004	0·002	0·001	0·002	0·005	0·004	0·002	0·012	0·005	0·012	0·005	0·001	0·002	0·000	0·001			
Al	0·377	0·429	0·517	0·444	0·356	0·523	1·614	1·551	1·543	1·983	2·089	1·967	1·922	1·953	2·384	2·534	2·333	0·973	0·967	0·963	0·974
Cr	0·004	0·000	0·001	0·002	0·000	0·000	0·011	0·003	0·004	0·007	0·002	0·005	0·001	0·001	0·011	0·002	0·005				0·001
Fe^{3+}	0·178	0·148	0·304	0·117	0·222	0·189	0·288	0·622	0·436				0·067	0·045				0·008	0·002	0·004	0·004
Fe^{2+}	0·057	0·119	0·089	0·103	0·117	0·116	0·843	0·986	1·087	0·148	0·224	0·228	1·605	1·741	1·328	2·557	1·864				
Mn	0·004	0·000	0·002	0·004	0·005	0·003	0·012	0·021	0·013	0·001	0·000	0·004	0·351	0·283	0·024	0·068	0·038				0·002
Mg	0·391	0·329	0·105	0·337	0·324	0·194	2·363	1·922	1·925	0·399	0·298	0·349	0·167	0·204	3·453	2·097	2·939	0·001			
Ca	0·444	0·417	0·136	0·431	0·399	0·246	0·066	0·143	0·076	0·000	0·001	0·004	0·876	0·772	0·001	0·003	0·002			0·001	0·005
Na	0·548	0·564	0·838	0·562	0·578	0·724	1·956	1·902	1·939	0·018	0·076	0·030	0·004	0·000	0·002	0·001	0·000	1·004	1·017	1·014	0·990
K	0·001	0·001	0·000	0·000	0·000	0·000	0·002	0·024	0·004	0·892	0·885	0·891	0·000	0·000	0·000	0·006	0·004	0·002	0·002	0·002	0·002
Total	4·000	4·000	4·000	4·000	4·000	4·000	15·095	15·024	15·004	6·954	7·005	6·977	8·000	8·000	10·004	10·002	10·010	5·000	5·007	5·006	4·993
X_{Mg}	0·872	0·735	0·542	0·767	0·735	0·627	0·737	0·661	0·639	0·730	0·570	0·605	0·094	0·105	0·722	0·451	0·612				
Jd	37·0	41·6	53·4	44·5	35·7	53·5															
Acm	17·8	14·8	30·4	11·7	22·2	18·9															
Aug	43·7	40·6	13·6	42·6	39·7	24·6															
Cat	0·7	1·1	0·0	0·5	0·2	0·0															

Omphacite calculated to six oxygens and four cations. Glaucophane calculated to 22 oxygens + 2 OH, Fe^{2+}/Fe^{3+} calculated after Schumacher (1997). Phengite calculated to 10 oxygens + 2 OH, total Fe as Fe^{2+}. Garnet calculated to 12 oxygens and eight cations. Chlorite calculated to 10 oxygens + 8 OH, total Fe as Fe^{2+}. Albite calculated to eight oxygens and total Fe as Fe^{3+}. $X_{Mg} = Mg/(Mg + Fe^{2+})$. Clinopyroxene end-members jadeite, acmite and augite after Morimoto *et al.* (1988).

of large tourmaline crystals (Fig. 3f), with only little omphacite and titanite and accessory allanite and rutile. Tourmaline crystals are about 5 mm in diameter and 30–50 mm in length, and show four zones in thin section. The cores (zone I) are light blue and sometimes contain inclusions of chlorite. The outer zones (II–IV) are free of inclusions and show greenish colours. Zone II is almost black and not developed in all grains. Zone III is dark green and the outermost zone IV is pale green.

Sample SY442 was taken from a blackwall wrapping an eclogite block with a thin black layer of tourmaline covering its surface (Fig. 3b). The blackwall is compositionally zoned with relatively sharp boundaries between the zones, changing with distance from the HP block. Sample SY442 was taken from a part consisting of omphacite and tourmaline crystals embedded in a matrix of albite (Fig. 3g and h). Tourmaline grains are 0·5–1·5 mm in diameter and 2–3 mm in length, and are concentrated in a layer of a few millimetres in thickness. They display four colour zones in thin section, with a light blue core (zone I), a green zone II, gradually fading into a dark, almost black zone III, which is sharply marked off from the green rim (zone IV; colours in plane-polarized light perpendicular to the *c*-axis; Fig. 3g). Omphacite inclusions are found in zones II–IV. Omphacite and albite ($Ab_{99·2}$) in the rock matrix are closely intergrown and show petrographic equilibrium in thin section, suggested by sharp and euhedral grain boundaries (Fig. 3h). Omphacite is chemically zoned, with type-1 cores characterized by low jadeite contents ($Jd_{36}Acm_{22}Q_{40}$) and type-2 rims with high jadeite contents ($Jd_{54}Acm_{19}Q_{25}$).

RESULTS

P–T conditions of formation of blackwalls and tourmaline

Temperature conditions during formation of tourmaline were calculated using the garnet–clinopyroxene Fe–Mg exchange thermometer, using the formulations by Ai (1994) and Krogh Ravna (2000), and by using THERMOCALC (v 3.01; Powell & Holland, 1988; Powell *et al.*, 1998). Only sample SY412 contains garnet in direct contact with type-2 omphacite, i.e. omphacite formed during the fluid influx that precipitated the tourmaline. Therefore, garnet–clinopyroxene thermometry was applied to garnet and type-2 omphacite in contact with one another in sample SY412 (Fig. 3e). The oxidation states of Fe in garnet and clinopyroxene were estimated by stoichiometric formula calculation. For an assumed pressure of 0·7 GPa, the thermometers of Ai (1994) and Krogh Ravna (2000) both give identical temperatures of 419°C. This is in agreement with the result from THERMOCALC (429°C). Accuracy of these calculated temperatures is not better than ±50°C,

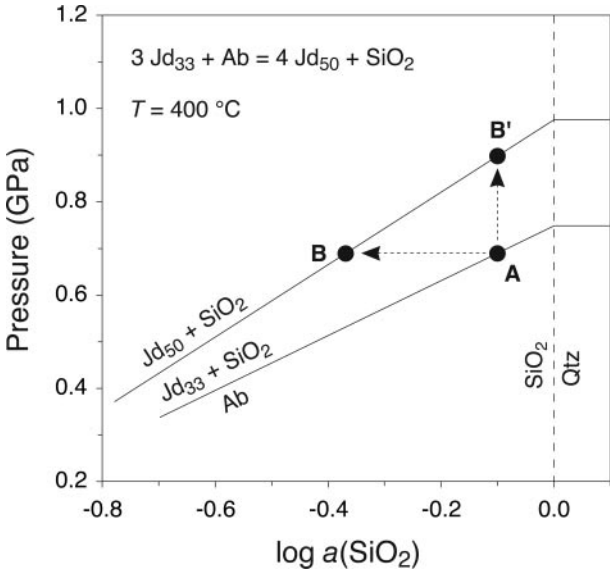

Fig. 4. *P*–log $a(SiO_2)$ diagram showing the upper pressure breakdown reaction of albite to omphacite + SiO_2 in the SiO_2-undersaturated field for pure albite and for omphacite with Jd_{33} and Jd_{50}.

as a result of uncertainties in the determination of the oxidation state of Fe, and the activity models for clinopyroxene and garnet, as well as the uncertainties of electron microprobe analyses.

Determining the pressure conditions during formation of the reaction zones is hampered by the fact that the samples are silica-undersaturated and quartz is generally absent. The breakdown reaction of albite,

$$Ab = Jd + SiO_2 \quad (1)$$

has often been used as a barometer for the calculation of minimum pressures in eclogitic rocks containing omphacitic clinopyroxene and quartz. The paragenesis albite + omphacite in the absence of quartz provides maximum pressures of equilibration only. However, reaction (1) is not only pressure (and temperature) sensitive, but can also act as a buffer reaction for SiO_2 during metasomatic processes. It has a positive slope in a *P*–log $a(SiO_2)$ diagram (Fig. 4). Addition of SiO_2 by a fluid entering a rock containing omphacite + albite at constant pressure would produce more albite by reducing the jadeite component of the coexisting clinopyroxene. Fluids undersaturated in SiO_2 with respect to the rock will remove SiO_2 from the mineral assemblage by decomposing albite and increasing the jadeite component in omphacite, as for example:

$$3Jd_{33} + Ab = 4Jd_{50} + SiO_2 \quad (2)$$

or

$$2CaMgSi_2O_6 + NaAlSi_2O_6 + NaAlSi_3O_8 = 2CaMgSi_2O_6 + 2NaAlSi_2O_6 + SiO_2. \quad (3)$$

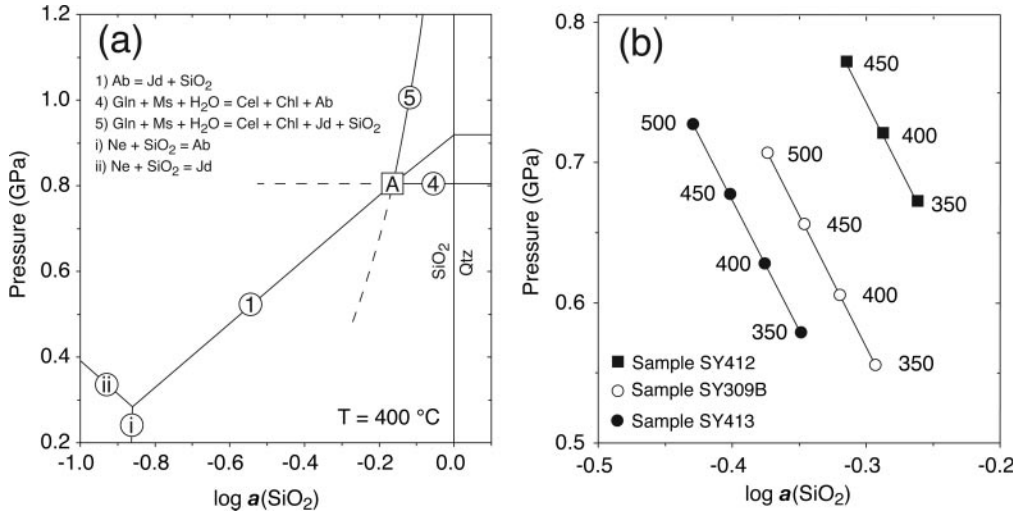

Fig. 5. (a) Schematic P – log $a(SiO_2)$ diagram showing the intersection of reactions (1), (4) and (5) in invariant point A. The reactions Ab = Ne + SiO_2 and Jd = Ne + SiO_2 are also shown. (b) Location of invariant point A calculated for samples SY309B (○), SY412 (■) and SY413 (●) in P – log $a(SiO_2)$ for different temperatures (given as numbers in °C).

Figure 4 shows the equilibria of albite + omphacite for two omphacites containing 33% and 50% jadeite, respectively. At constant temperature, reaction (2) could shift an assemblage from point A to point B by reducing $a(SiO_2)$ or proceed to point B′ by increasing pressure. Omphacite in several samples (SY327, SY412, SY442) shows a two-stage zonation, with cores of low jadeite ($Jd_{36–42}$) and rims of high jadeite ($Jd_{52–54}$) contents. Assuming constant pressure, the first fluid had a higher silica activity, stabilizing Jd_{33} + Ab (point A in Fig. 4), whereas the second fluid had a significantly lower $a(SiO_2)$, producing Jd_{50} + Ab (point B in Fig. 4). The Ab + Omp equilibrium for a specific omphacite composition is shifted to higher pressures for higher SiO_2 activities and reaches maximum pressures at $a(SiO_2) = 1$ (i.e. in the presence of quartz). Therefore, a second, independent equilibrium is needed to determine pressure and silica activity during tourmaline formation.

Samples SY309B, SY413 and SY412 show the mineral assemblage glaucophane + phengite + albite + chlorite + omphacite in equilibrium with tourmaline. The equilibrium of glaucophane, phengite, chlorite and albite or jadeite was calculated by the reactions

$$\mathrm{Gln + Ms + H_2O = Cel + Chl + Ab} \quad (4)$$

$$\mathrm{Gln + Ms + H_2O = Cel + Chl + Jd + SiO_2}. \quad (5)$$

Figure 5a shows the calculated locations of reactions (1), (4) and (5) in a P–log $a(SiO_2)$ diagram, intersecting at the invariant point A at an assumed temperature of 400°C. Figure 5b displays the location of point A in the P–log $a(SiO_2)$ field for different temperatures and compositions. For a temperature of 400°C, point A is located at pressures of 0·61, 0·63 and 0·72 GPa for samples SY309B, SY413 and SY412, respectively. Silica activities in the three samples are 0·48 [SY309B; log $a(SiO_2)$ = −0·32], 0·42 [SY413; log $a(SiO_2)$ = –0·38] and 0·51 [SY412; log $a(SiO_2)$ = –0·29].

In accordance with other workers (Trotet *et al.*, 2001*b*; Rosenbaum *et al.*, 2002; Putlitz *et al.*, 2005) we conclude that the Syros rocks were exhumed along a near-isothermal decompression path; that is, showing a temperature decrease of ≤100°C during decompression to ∼0·6 GPa. During exhumation of the unit, reaction zones formed at contacts between the contrasting lithologies, partly enhanced by mechanical mixing but also triggered by a strong influx of hydrous fluids, which reduced the activity of SiO_2 in the rocks to values between 0·4 and 0·5. Reaction zones (blackwalls) are dominated by hydrous minerals such as chlorite, glaucophane, phengite, talc and Ca-amphibole, and contain abundant tourmaline that was precipitated during the formation of the blackwalls. P–T conditions of tourmaline formation were 400–430°C and 0·62–0·72 GPa (Fig. 6). Therefore, a major influx of boron-rich hydrous fluid into the Syros mélange must have occurred during exhumation of the unit at a depth of 20–25 km.

Chemical composition of blackwall tourmaline

Apart from X_{Mg}, variation of tourmaline chemical composition between the samples is very limited (Table 3). Formula calculations based on 31 oxygens and total Fe as Fe^{2+} result in 5·86–5·99 Si, 5·82–6·09 Al,

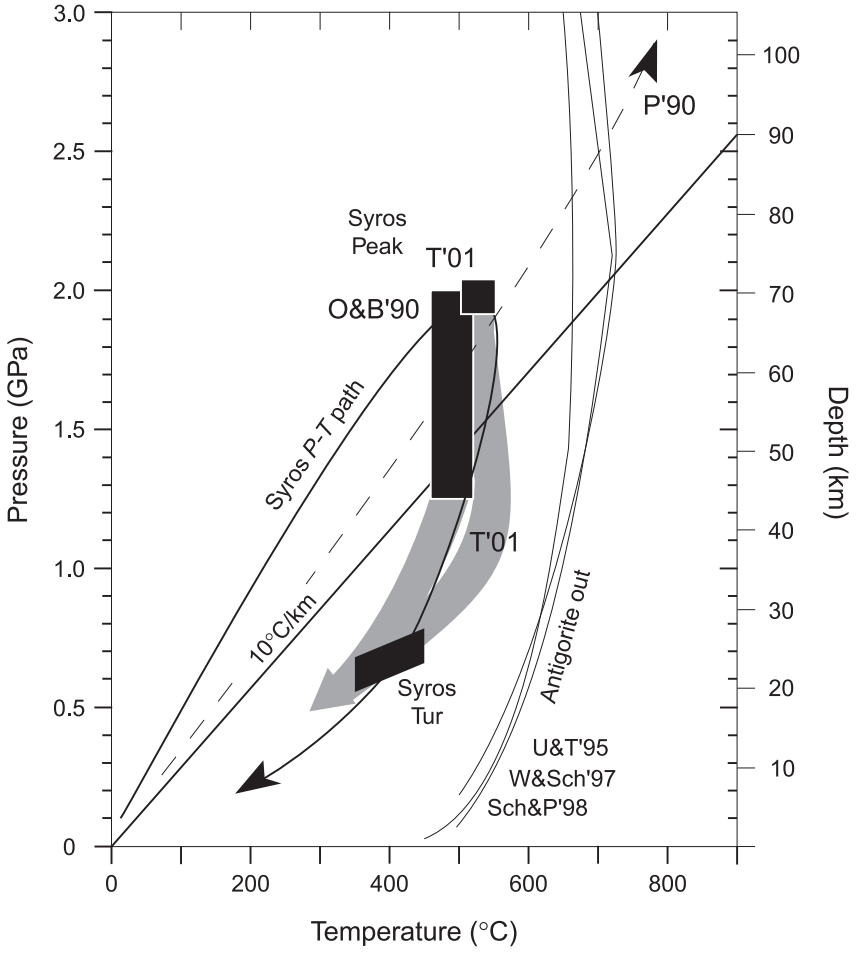

Fig. 6. *P–T* diagram showing the prograde and retrograde *P–T* path of Syros HP rocks. Peak conditions were taken from Okrusch & Bröcker (1990) and Trotet *et al.* (2001*b*). Conditions of tourmaline formation were determined during this study. The grey arrows mark retrograde *P–T* paths for Syros eclogites and blueschists taken from Trotet *et al.* (2001*b*). The upper thermal stability limit of antigorite, experimentally determined by several workers (Ulmer & Trommsdorff, 1995; Wunder & Schreyer, 1997; Schmidt & Poli, 1998), was not reached in the rocks from Syros. P'90 is the *P–T* path B for subducting slabs from Peacock (1990). The continuous line is a 10°C/km geothermal gradient.

3·05–3·17 B and 2·93–3·25 (Mg + Fe + Ti) per formula unit. Syros blackwall tourmaline analysed in an earlier study showed a $Fe^{3+}/\Sigma Fe$ ratio of ~0·30 (Marschall *et al.*, 2004). TiO_2 contents are between 0·12 and 1·14 wt % and vary between the zones of the crystals that were distinguished by colour in thin section. Ti contents are lowest in the light blue cores and higher in the dark green zones. The X-site is (almost) completely occupied by Na [0·92–0·98 cations per formula unit (c.p.f.u.)] and only minor Ca (0·01–0·05 c.p.f.u.). Analyses of F, Cl and H contents revealed no detectable Cl, very minor F (<0·03 p.f.u.) and high OH contents, >3·75 OH p.f.u., in most cases. Cr_2O_3 contents range from 0 to 0·28 wt %, which translates to ≤0·04 c.p.f.u. Cr. All other elements measured are of negligible concentrations in the tourmalines, including Mn, Zn, K and Li. Boron contents in excess of 3·00 c.p.f.u. in dravite, as well as high Na and OH contents, have been discussed by Marschall *et al.* (2004). The calculated formulae are very close to the ideal schorl–dravite solid solution series and belong to the alkali-dravite group of Hawthorne & Henry (1999) with X_{Mg} between 0·58 and 0·82. Blue cores generally have higher X_{Mg} than green rims, with positive correlation of Fe, Ti and Ca contents.

Boron isotopic composition of blackwall tourmaline

The small size of the SIMS spot during determination of B isotope ratios in tourmaline (≤5 μm) allows us to measure very detailed profiles even in small grains, and to unravel small-scale isotopic heterogeneities. During this study, traverses with 10–50 spots each were obtained for all eight samples.

Table 3: Chemical and B isotopic analyses of tourmaline

Sample:	SY309B		SY327		SY400		SY412		SY413		SY420		SY441				SY442			
Type:	core	rim	core	rim	core	rim	core	rim	core	rim	core	rim	core	zone II	zone III	zone IV	core	zone II	zone III	zone IV
SiO_2	36·10	35·75	35·57	35·68	36·27	36·08	35·98	35·51	35·87	35·31	36·21	35·85	36·25	36·18	36·48	36·38	36·09	35·79	35·92	35·57
TiO_2	0·12	0·56	1·14	0·57	0·44	0·11	0·16	0·79	0·49	0·68	0·16	0·59	0·12	0·75	0·48	0·44	0·17	0·49	0·63	0·72
B_2O_3	11·05	10·75	10·58	10·73	11·18	11·16	10·74	10·64	10·60	10·55	11·07	10·84	11·12	11·14	11·15	11·31	11·00	11·01	10·88	10·87
Al_2O_3	31·26	30·39	29·53	30·59	31·35	31·78	30·58	29·41	30·10	29·68	30·79	30·00	31·41	30·31	31·17	31·20	31·00	30·18	29·89	29·62
Cr_2O_3	0·19	0·28	0·04	0·00	0·09	0·01	0·00	0·00	0·06	0·09	0·02	0·02	0·00	0·00	0·03	0·01	0·10	0·09	0·01	0·01
FeO^t	5·13	6·85	9·17	7·58	4·61	3·94	7·64	9·28	7·30	8·76	5·54	6·78	4·60	5·99	4·97	4·12	5·97	7·68	8·48	8·41
MnO	0·00	0·00	0·00	0·00	0·01	0·03	0·00	0·02	0·01	0·00	0·03	0·04	0·03	0·03	0·00	0·04	0·04	0·00	0·02	0·00
MgO	9·21	8·53	7·21	7·89	9·31	9·95	8·24	7·39	8·39	7·67	9·27	8·84	9·73	9·25	9·28	9·78	8·83	8·29	7·81	7·75
CaO	0·10	0·27	0·25	0·22	0·21	0·07	0·14	0·28	0·23	0·25	0·11	0·24	0·09	0·28	0·26	0·18	0·14	0·25	0·28	0·21
ZnO	0·03	0·00	0·00	0·00	0·00	0·03	0·00	0·03	0·04	0·05	0·04	0·00	0·01	0·03	0·00	0·01	0·06	0·00	0·00	0·00
Na_2O	3·08	3·04	2·92	2·96	2·94	3·12	3·03	2·84	2·96	3·00	3·03	2·96	3·03	2·96	2·97	2·99	2·92	2·94	3·00	2·94
K_2O	0·02	0·00	0·00	0·02	0·03	0·01	0·03	0·01	0·04	0·02	0·04	0·03	0·01	0·02	0·00	0·01	0·04	0·03	0·04	0·03
Li (μg/g)	2·0	2·1	8·5	6·9	6·0	6·7	4·0	5·0	4·6	4·4	4·1	4·7	4·6	3·1	3·8	6·0	5·1	5·8	8·0	6·7
H_2O	3·78	3·59	3·32	3·39	3·75	3·62	3·41	3·27	3·20	3·17	3·62	3·27	3·66	3·54	3·57	3·64	3·46	3·53	3·32	3·20
F	0·04	0·04	0·03	0·05	0·05	0·02	0·02	0·04	0·01	0·05	0·00	0·06	0·00	0·03	0·02	0·02	0·04	0·03	0·02	0·06
Cl	0·01	0·01	0·00	0·00	0·00	0·01	0·00	0·00	0·01	0·00	0·00	0·00	0·02	0·00	0·00	0·00	0·01	0·00	0·01	0·02
-(F + Cl) = O	0·02	0·02	0·01	0·02	0·02	0·01	0·01	0·02	0·01	0·02	0·00	0·03	0·00	0·01	0·01	0·01	0·02	0·01	0·01	0·03
Total	100·10	100·05	99·75	99·66	100·22	99·91	99·96	99·50	99·32	99·24	99·91	99·49	100·07	100·49	100·38	100·12	99·84	100·30	100·32	99·38
Formulae calculated to 31 oxygens, $Fe^{2+} = Fe^t$																				
Si	5·88	5·90	5·96	5·92	5·88	5·86	5·96	5·96	5·99	5·94	5·93	5·95	5·90	5·91	5·93	5·90	5·93	5·90	5·96	5·95
Ti	0·02	0·07	0·14	0·07	0·05	0·01	0·02	0·10	0·06	0·09	0·02	0·07	0·01	0·09	0·06	0·05	0·02	0·06	0·08	0·09
B	3·11	3·06	3·06	3·08	3·13	3·13	3·07	3·08	3·05	3·07	3·13	3·11	3·12	3·14	3·13	3·17	3·12	3·13	3·12	3·14
Al	6·00	5·91	5·83	5·99	5·99	6·09	5·97	5·82	5·92	5·89	5·94	5·87	6·02	5·84	5·97	5·96	6·00	5·86	5·84	5·84
Cr	0·03	0·04	0·01	0·00	0·01	0·00	0·00	0·00	0·01	0·01	0·00	0·00	0·00	0·00	0·00	0·00	0·01	0·01	0·00	0·00
Fe^{2+}	0·70	0·95	1·28	1·05	0·63	0·54	1·06	1·30	1·02	1·23	0·76	0·94	0·63	0·82	0·68	0·56	0·82	1·06	1·18	1·18
Mn	0·00	0·00	0·00	0·00	0·00	0·00	0·00	0·00	0·00	0·00	0·00	0·01	0·00	0·00	0·00	0·01	0·01	0·00	0·00	0·00
Mg	2·24	2·10	1·80	1·95	2·25	2·41	2·03	1·85	2·09	1·93	2·26	2·19	2·36	2·25	2·25	2·36	2·16	2·04	1·93	2·93
Ca	0·02	0·05	0·05	0·04	0·04	0·01	0·03	0·05	0·04	0·05	0·02	0·04	0·02	0·05	0·05	0·03	0·02	0·05	0·05	0·04
Zn	0·00	0·00	0·00	0·00	0·00	0·00	0·00	0·00	0·01	0·01	0·00	0·00	0·00	0·00	0·00	0·00	0·01	0·00	0·00	0·00
Na	0·97	0·97	0·95	0·95	0·93	0·98	0·97	0·92	0·96	0·98	0·96	0·95	0·96	0·94	0·94	0·94	0·93	0·94	0·97	0·96
K	0·01	0·00	0·00	0·00	0·01	0·00	0·01	0·00	0·01	0·00	0·01	0·01	0·00	0·00	0·00	0·00	0·01	0·01	0·01	0·01
Total	18·96	19·03	19·07	19·06	18·92	19·04	19·10	19·11	19·16	19·19	19·03	19·14	19·02	19·04	18·99	18·98	19·04	19·06	19·13	19·14
X_{Mg}	0·762	0·689	0·584	0·650	0·783	0·818	0·658	0·587	0·672	0·610	0·749	0·699	0·790	0·734	0·769	0·809	0·725	0·658	0·621	0·622
OH	4·11	3·95	3·71	3·76	4·06	3·92	3·78	3·66	3·56	3·56	3·95	3·62	3·97	3·86	3·87	3·94	3·79	3·88	3·67	3·57
F	0·02	0·02	0·02	0·03	0·03	0·01	0·01	0·02	0·00	0·03	0·00	0·03	0·00	0·02	0·01	0·01	0·02	0·02	0·01	0·03
Cl	0·00	0·00	0·00	0·00	0·00	0·00	0·00	0·00	0·00	0·00	0·00	0·00	0·00	0·00	0·00	0·00	0·00	0·00	0·00	0·01
Total	4·13	3·97	3·72	3·78	4·08	3·94	3·79	3·68	3·57	3·59	3·95	3·65	3·97	3·88	3·88	3·95	3·82	3·90	3·69	3·61
Boron isotope values determined by SIMS																				
$\delta^{11}B$	21·6	21·6	21·7	21·8	19·0	20·3	21·2	20·8	22·2	21·4	20·0	20·0	18·8	18·3	19·1	19·3	28·4	27·9	28·3	21·9
$2RSD_{mean}$	0·8	1·0	0·9	1·1	1·2	0·8	1·6	1·5	1·5	2·2	1·8	0·9	0·9	-	0·9	0·9	0·7	2·6	1·4	3·0
n	12	10	5	6	18	9	4	9	14	18	3	7	3	1	4	4	5	17	8	18

$\delta^{11}B$ values are mean values of all SIMS isotope analyses (displayed in Fig. 7). *n*, number of isotope analyses. H (H_2O), Li and B measured by SIMS; all other elements by EPMA.

JOURNAL OF PETROLOGY VOLUME 47 NUMBER 10 OCTOBER 2006

The results of these measurements show four important features, as follows.

(1) $^{11}B/^{10}B$ isotopic ratios are very high, exceeding $\delta^{11}B$ values of +18‰ in all samples, with an extreme value of +28·4 ± 0·7‰ (2σ) in the tourmaline core of sample SY442 (Table 3, Fig. 7h).

(2) In seven out of eight samples intra-grain variation of $\delta^{11}B$ is very limited, with profiles showing very little or a lack of internal zonation (Fig. 7). Differences between core and rim values are within analytical uncertainties (Table 3).

(3) Variation of $\delta^{11}B$ between these seven different samples is also weak, ranging from +18·8 ± 0·9‰ (sample SY441) to +22·2 ± 1·5‰ (sample SY413).

(4) Sample SY442 is different from the other seven samples, as it displays a strong zonation in $\delta^{11}B$ (Fig. 7h), which correlates with the optically visible zones (Fig. 3g). The blue core as well as zones II and III are extremely enriched in the heavy isotope, with $\delta^{11}B$ values of ~+28‰ (Table 3), whereas zone IV is significantly lighter. There is a sharp jump of ~6‰ within 10 μm at the boundary between zones III and IV. Zone IV itself displays an internal isotopic zonation with $\delta^{11}B$ increasing from +21·5‰ in contact with zone III, to +24·0‰ in the centre of zone IV, to ~+20·0‰ at the edge of the tourmaline (Fig. 7h). A more detailed discussion of the $\delta^{11}B$ profile in this sample is given below.

DISCUSSION

Boron concentration of blackwall-forming fluids

As no data on fluid inclusions related to the tourmaline-forming 'event' are available, the concentration of B in the fluids can be estimated only indirectly from B concentrations in minerals. Omphacitic clinopyroxene formed together with tourmaline from different samples within the blackwalls contains between 1·92 μg/g (SY309B) and 3·28 μg/g (SY441) B (Marschall, 2005). Combined with the clinopyroxene–fluid partition coefficient of 0·016 determined by Brenan *et al.* (1998*b*), these abundances would imply B concentrations of the fluids in the range of 120–205 μg/g. Experimental studies by Morgan & London (1989) have shown that crystallization of tourmaline from solutions containing <0·2 wt % B_2O_3 (620 μg/g B) is possible, provided the fluids are low in pH (pH of quenched fluids <6·5). Morgan & London also demonstrated that tourmaline is not stable in alkaline fluids (pH >6·5) regardless of B concentration. Weisbrod *et al.* (1986) (cited by Dingwell *et al.*, 2002) were able to crystallize dravite from Fe-free chlorite-bearing compositions in equilibrium with fluids containing between ~150 μg/g and ~300 μg/g B, in the temperature range of 350–450°C. This may indicate that the calculated B concentrations of ~100–200 μg/g are not too low for the formation of tourmaline.

Fractionation of boron isotopes

Theoretical calculations of isotope fractionation of boron predict preference of ^{10}B for crystallographic sites tetrahedrally coordinated to oxygen, and ^{11}B for trigonal sites. B in acidic hydrous fluids is predominantly trigonally coordinated in $B(OH)_3$ units. Recent experiments have shown that this also holds true for high pressures up to 2·0 GPa (Schmidt *et al.*, 2005). Boron in tourmaline is also typically trigonally coordinated with three BO_3 groups per formula unit. Only small amounts of tetrahedral B were observed in tourmaline from Syros (Marschall *et al.*, 2004), ranging from 0·1 to 0·2 B c.p.f.u. Therefore, at least 95% of the B in Syros tourmaline is trigonally coordinated. The tourmaline-forming hydrous fluid must have been acidic to stabilize tourmaline and, therefore, contained B in trigonal coordination $[B(OH)_3]$.

Experimental studies (e.g. Hervig *et al.*, 2002 and references therein; Heinrich *et al.*, 2003; Wunder *et al.*, 2004; Sanchez-Valle *et al.*, 2005) have investigated the temperature dependence of B isotopic fractionation between phases of different B coordination (e.g. mica, amphibole, melt, fluid, tourmaline). Hervig *et al.* (2002) demonstrated a systematic decrease of fractionation with increasing temperature between phases containing tetrahedrally and trigonally coordinated boron, respectively, given by the formula

$$1000 \ln \alpha = 5{\cdot}68 - 12290/T \qquad (6)$$

where α is the fractionation factor and T is absolute temperature (K). For a temperature of 400°C, the assumed temperature for Syros blackwall formation, a fractionation of 12·6‰ between phengite and fluid or phengite and tourmaline results from this equation. Applying the formulations of other researchers to this example results in very similar isotope fractionations of 12·6‰ (Williams *et al.*, 2001) and 12·0‰ (Wunder *et al.*, 2004). We applied the formulation of Hervig *et al.* (2002), as it is based on the largest dataset, including natural and synthetic systems. The fractionation between tourmaline (0·15 B^{IV} c.p.f.u.) and fluid would be 0·6‰ applying equation (6), assuming that equilibrium fractionation is exclusively determined by the coordination of B in the phases. However, Palmer *et al.* (1992) have demonstrated experimentally a fractionation between tourmaline and fluid of ~4·5‰ at 400°C and 0·2 GPa, which decreases with both increasing temperature and pressure.

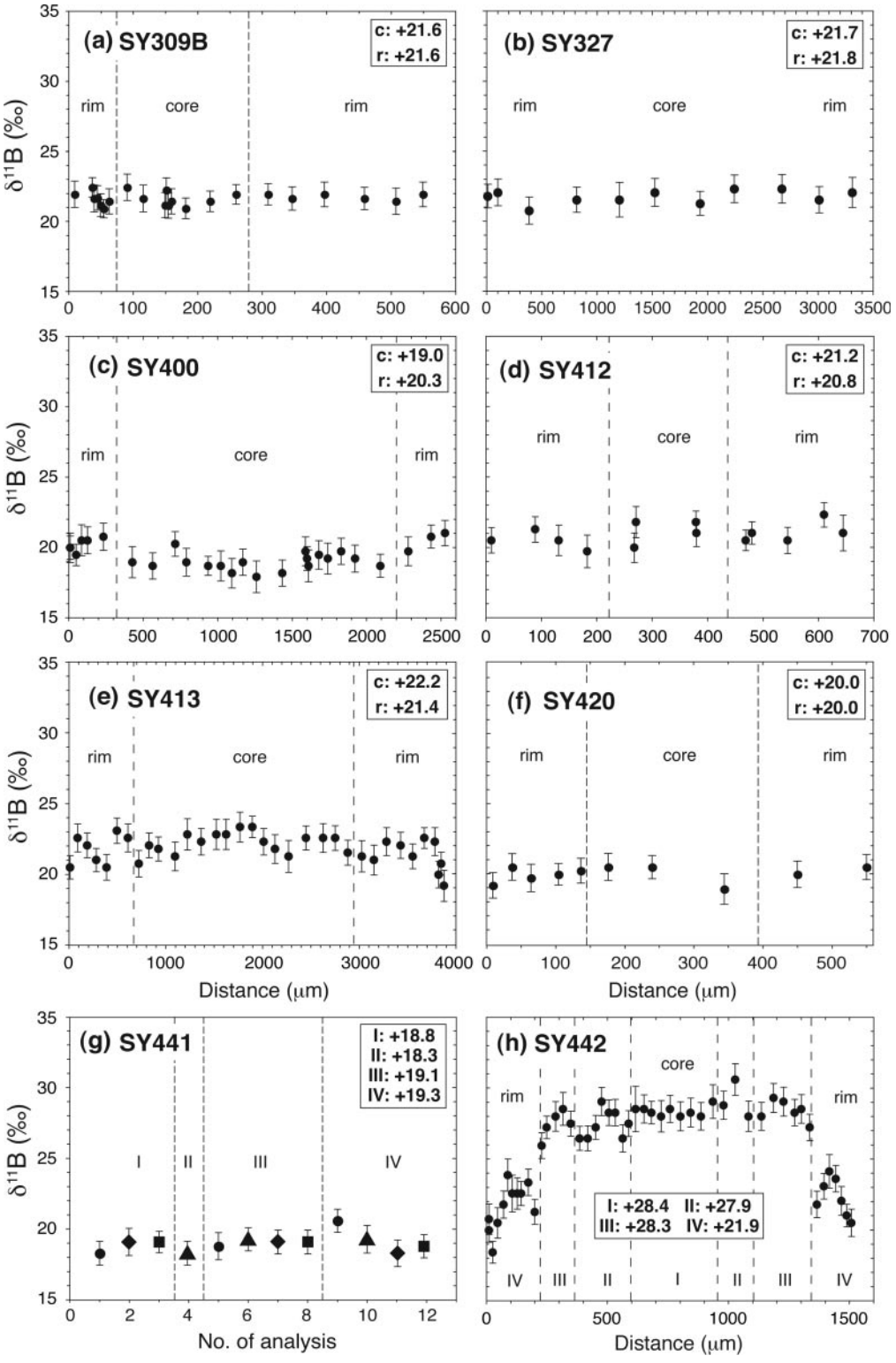

Fig. 7. Results of SIMS analyses of B isotopic composition of tourmaline from Syros. For each sample, at least one traverse of 10–50 single spot analyses was carried out across a grain. Average $\delta^{11}B$ values are given by the numbers in the boxes. Error bars give analytical precision as $2RSD_{mean}$. (a) Sample SY309B; (b) sample SY327; (c) sample SY400; (d) sample SY412; (e) sample SY413; (f) sample SY420; (g) sample SY441. In sample SY441, no profile over one single grain was measured, but analyses from several grains (indicated by different symbols) were collected and sorted by location (zone I– IV) within the crystals. (h) Sample SY442.

Tourmaline from this study shows very homogeneous δ^{11}B values even in large grains. As these grains were precipitated from hydrous fluid(s) entering the rocks, boron isotopic fractionation processes between the two phases can be monitored using these samples. The formation of tourmaline containing ~30 000 μg/g B significantly decreases the B concentration of any coexisting fluid. At low fluid/rock ratios, isotopic fractionation between tourmaline and fluid, as described by Palmer *et al.* (1992), would lead to an increase of δ^{11}B in the fluid over time and consequently to an isotopic zonation within the precipitated tourmaline grains, with δ^{11}B values increasing from cores to rims. Flat δ^{11}B patterns can be explained either (1) by a very high fluid/rock ratio, flushing the reaction zones with fluid of constant δ^{11}B, or (2) by weak or absent B isotopic fractionation between tourmaline and hydrous fluid at the *P–T* conditions of interest. Some of the investigated samples indeed show evidence for high fluid/rock ratios, as they contain large amounts of chlorite and no relics of their primary parageneses. Those samples are located at the outermost parts of the high-pressure blocks (SY441), or in the matrix (SY309B). However, SY412 was sampled from the core of an eclogite block that shows a gradual transition into blueschist and finally a chlorite-rich assemblage at its rim. SY412 still shows high proportions of its eclogitic paragenesis (Grt + Omp I + Rt), and only restricted hydration. This sample also contains large tourmaline grains with flat δ^{11}B patterns (Fig. 7d). The petrographical observations suggest that (1) fluid/rock ratios strongly decreased from the matrix of the Syros mélange to the cores of the high-pressure blocks, and (2) fluid/rock ratios were rather low during retrogression of eclogite SY412, but significantly increased towards the block's rim (sample SY413). Fluid supply in the eclogitic core of the block was limited and the growing tourmaline must have had a strong impact on the B concentration of the fluid. Any isotopic fractionation between tourmaline and fluid would, therefore, have been documented in the precipitated tourmaline grains. The flat δ^{11}B patterns in sample SY412 can, thus, only be explained by negligible B isotopic fractionation between tourmaline and hydrous fluid. This is in agreement with the fact that B in both tourmaline and acidic hydrous fluids is predominantly in trigonal coordination. In addition, Tonarini *et al.* (1998) reported δ^{11}B values of tourmaline precipitated in miarolitic dykes on Elba island (Italy). Those workers suggested negligible B isotopic fractionation between tourmaline and fluid as a possible explanation for the absence of any significant B isotopic zonation within the tourmaline. However, these suggestions are in contrast to the experimental study of Palmer *et al.* (1992) at a pressure of 0·2 GPa.

B isotopic zonation in tourmaline of sample SY442

The strong B isotopic zonation in tourmaline of sample SY442 cannot be explained by fractionation effects between fluid and minerals during formation of the sample or by temperature effects. Instead, the zoning must be due to the precipitation of tourmaline from two different fluids of isotopically different composition entering the rock one after the other. This hypothesis is supported by the two-stage zonation of omphacite in this sample, showing the influx of a second fluid also leading to a drop in SiO_2 activity. Omphacite in the matrix shows a two-stage zonation with cores of Jd_{36} and rims of Jd_{53}. Omphacite included in tourmaline zones II and III (Fig. 3g) is relatively low in Na (Jd_{33}), whereas the rims of omphacite included in tourmaline zone IV are high in Na (Jd_{45}). Therefore, the two different omphacite generations can be related to different fluid pulses and growth stages of tourmaline, with a higher silica activity in the first fluid and a significantly lower $a(SiO_2)$ in the second fluid. Inclusions of type-1 omphacite in tourmaline zones I, II and III (high δ^{11}B) and inclusions of type-2 omphacite occurring exclusively in zone IV, characterized by lower δ^{11}B, support a genetic relationship between the two omphacite generations and the tourmaline generations. In some places, zone III is corroded and replaced by zone IV (Fig. 3g), suggesting that parts of the previously grown high-δ^{11}B tourmaline were dissolved during influx of the lower-δ^{11}B second fluid. This must have led to local mixing of B from the early tourmaline and the later fluid with their two contrasting isotopic compositions. The internal isotopic zonation of zone IV (Fig. 7h) is, therefore, best explained by mixing between B with $\delta^{11}B \sim +28‰$ from early tourmaline and B with $\delta^{11}B \sim +20‰$ from the second fluid. Hence, sample SY442 provides evidence for two fluids of different compositions.

Possible source of ^{11}B-rich fluid

The formation of centimetre- to metre-sized reaction zones rich in OH-bearing minerals including tourmaline at 20–30 km depth during exhumation requires large amounts of H_2O and boron. Within the mélange itself, there are no appreciable sources of H_2O, because the metabasic rocks were already dehydrated on the prograde path, and because OH-bearing minerals in carbonates and schists, such as glaucophane and mica, survived the peak and retrograde metamorphism. Furthermore, the upper thermal stability of antigorite was not reached at Syros (Fig. 6). Thus, serpentinite, which is, in principle, an important carrier of H_2O, did not dehydrate. In addition, the fact that the low δ^{11}B values of minerals from the Syros high-pressure rocks were not significantly affected by late-stage fluid

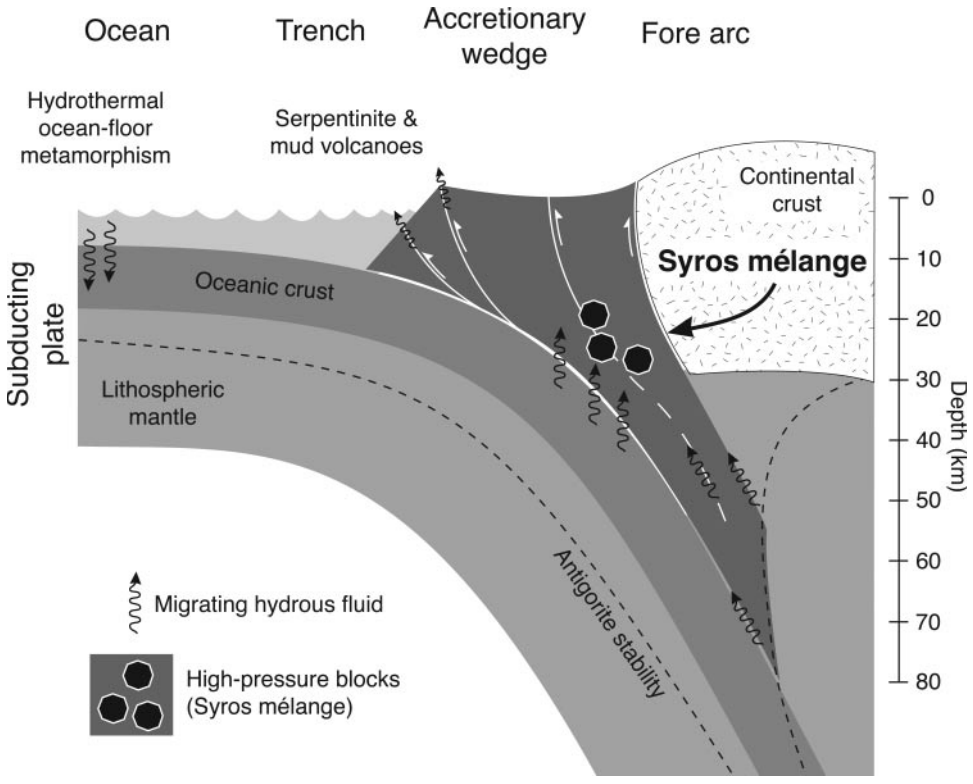

Fig. 8. Sketch of vertical cross-section through a subduction zone showing the exhumation channel located between the subducting slab on the left and the overlying plate on the right. High-pressure rocks, now exposed on the island of Syros, were rehydrated during their exhumation by aqueous fluids, probably released from the progressively subducted slab.

infiltration (Marschall, 2005) rules out these rocks as a boron source for tourmaline formation. Phengite ($\delta^{11}B = -11{\cdot}3 \pm 1{\cdot}4‰$) and metamorphic tourmaline ($\delta^{11}B = +0{\cdot}9 \pm 1{\cdot}8‰$) in a siliceous marble, antigorite ($\delta^{11}B = +0{\cdot}4 \pm 7{\cdot}8‰$) from a serpentinite, tourmaline from an eclogite ($\delta^{11}B = +2{\cdot}8 \pm 1{\cdot}0‰$), and metamorphic tourmaline from a metasedimentary schist ($\delta^{11}B = -1{\cdot}6 \pm 1{\cdot}1‰$) from the Syros mélange (Marschall, 2005) all show that the fluids in equilibrium with these rocks would have had $\delta^{11}B$ values between –3 and +3‰ (marble, schist and eclogite) or about +13‰ (acidic fluid in isotopic equilibrium with serpentinite at 400°C), significantly lower than that required for blackwall formation. Thus, it is concluded that H_2O and boron were introduced into the mélange from external sources.

Modern subduction zone models involve a wedge or channel of exhuming rocks, which is located between the subducting and the overriding plate (Shreve & Cloos, 1986; Liou *et al.*, 1997; Engi *et al.*, 2001; Ernst, 2001; Guillot *et al.*, 2001; Rubatto & Hermann, 2001; Gerya *et al.*, 2002; Ring & Fleischmann, 2002; Roselle & Engi, 2002; Jolivet *et al.*, 2003). Slices of HP rocks, sheared off from the subducting plate and tectonically mixed with serpentinites from the hanging wall, may rapidly ascend in these exhumation channels, while the subduction system is still active. Therefore, fluids released from the subducting plate will enter the overlying exhumation channel and rehydrate the HP rocks on their way back to the surface. The source of the B-rich fluids fluxing into the Syros mélange is probably also located within the plate, which continued to subduct during the exhumation of the Syros mélange (Fig. 8).

Boron budget of fluids and rocks during dehydration

Major hosts of B in oceanic crust prior to subduction are low-temperature altered basalts and serpentinites that interacted with seawater at low temperatures, sediments (including pore water within the sediments) and altered basalts. B, therefore, is stored in the uppermost part of the subducting slab in the same reservoirs that contain most of the slab water. However, among these reservoirs, high $\delta^{11}B$ values (>+5‰) are likely only in pore water, low-temperature altered basalts or serpentinites. B in altered basalts is mainly stored in clay minerals, either in their crystal structures or adsorbed on their surfaces (Harder, 1970; You *et al.*, 1996*b*; Williams *et al.*, 2001). This leads to (1) the loss of B during diagenesis and early

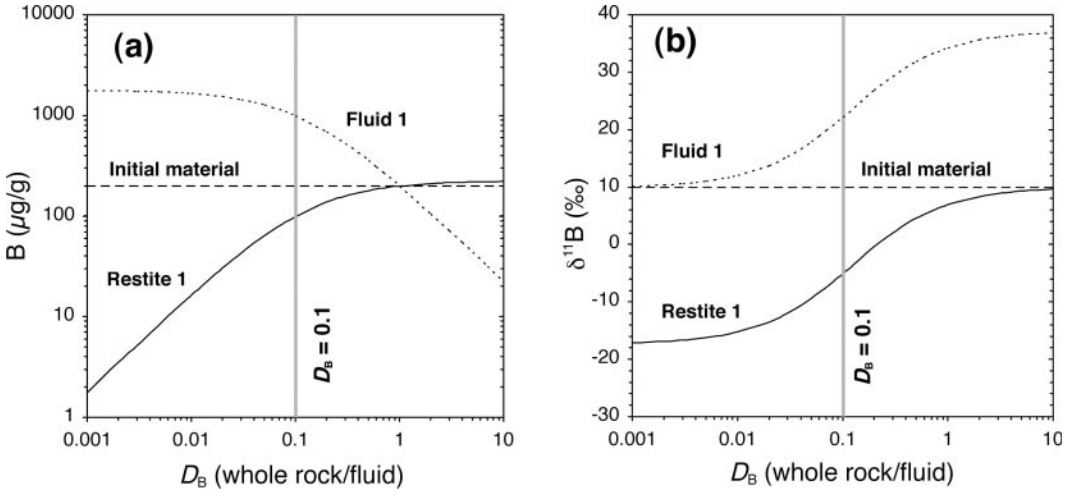

Fig. 9. (a) Calculated B concentrations in the initial material (dashed line), restitic material (continuous line) and escaping fluid (dotted line) for batch dehydration as a function of whole-rock–fluid B partition coefficient D_B. Vertical grey line marks a partition coefficient D_B of 0·1. (b) δ^{11}B value vs whole-rock–fluid B partition coefficient, showing the calculated B isotopic composition of initial material (dashed line), restitic material (continuous line) and escaping fluid (dotted line). Vertical grey line marks partition coefficient D_B of 0·1. Calculations are based on the following parameters for the first dehydration step: H_2O content decreasing from 20 to 10 wt %; B concentration in initial rock 200 μg/g; $\delta^{11}B = +10‰$; $T = 100°C$.

metamorphism and (2) the release of major amounts of B during the onset of subduction, as discussed by Leeman & Sisson (2002). Loss of pore water, adsorbed and crystalline water from low-grade minerals (clay minerals) at temperatures below 150°C will lead to a decrease of B concentrations within the subducting material at an early stage. The evolution of the B isotopes during dehydration depends on the pH of the released fluid. Basic fluids will have a B isotope composition identical to that of the silicates in the dehydrating rocks from which they originated, as all these phases contain boron in tetrahedral coordination. In contrast, acidic fluids will strongly fractionate the B isotopes. They will show high δ^{11}B values at the onset of dehydration and lead to progressively decreasing δ^{11}B values within the subducting rocks.

To model the B isotope fractionation during dehydration, an average partition coefficient of B between acidic hydrous fluid and restitic rock is required, as well as the temperature-dependent B isotopic fractionation, water and B contents and B isotopic composition of the rock prior to subduction. In this study, the isotopic fractionation given by equation (6) is used. For the composition of the initial rock, high δ^{11}B values (+10‰) and B concentrations (200 μg/g) were assumed, both at the high end of the range observed in low-temperature altered oceanic basalts and in clay-rich sediments. Whole-rock–fluid partition coefficients for B are not published in the literature and have to be estimated as discussed below.

Figure 9 shows the B concentration (Fig. 9a) and B isotopic composition (Fig. 9b) of fluid and restitic rock as functions of the whole-rock–fluid partition coefficient D_B during dehydration of an initial rock with the above-mentioned composition. In principle, three areas should be distinguished in Fig. 9, with respect to D_B, as follows. (1) In the range of high mobility (D_B ~0·001–0·01) almost all B leaves the rock, producing a B-rich fluid and a nearly B-free restite. The B isotopic composition of the fluid is similar to that of the initial rock (+10‰ in this case). (2) In the range of immobile behaviour ($D_B > 1$), the B concentration and isotopic composition of the restite are similar to that of the initial rock, whereas the fluid shows a very high δ^{11}B value, but a rather low concentration of B. (3) The range of moderate B mobility (D_B 0·01–1) produces a fluid with both a high δ^{11}B value and a high B content along with a restite with moderate B concentration and a δ^{11}B value significantly lower than that of the initial rock. It is generally accepted that significant amounts of B are lost during diagenesis and the early stages of metamorphism and that B is readily transported by hydrous fluids (Moran *et al.*, 1992; Bebout, 1996; Leeman, 1996; You *et al.*, 1996*a*; Bebout *et al.*, 1999; Deyhle & Kopf, 2002; Kopf & Deyhle, 2002). Therefore, we assume low whole-rock–fluid partition coefficients between 0·01 and 0·1 to calculate the B budget and isotopic composition of acidic fluids and rocks during dehydration.

The results of the calculations are displayed in Fig. 10. The first fluids are characterized by both high B concentrations and δ^{11}B values, as would be expected from a water- and B-rich source (20 wt % H_2O, 200 μg/g B). However, subsequently released acidic fluids show δ^{11}B values below +10‰ (Fig. 10); that is,

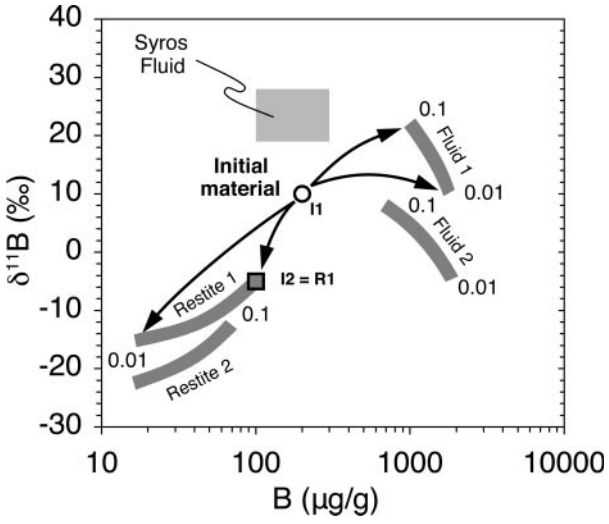

Fig. 10. Model $\delta^{11}B$ values and B concentrations reached in restitic material and released fluid during dehydration. Grey arrays define ranges of results for rock–fluid partition coefficients (D_B) between 0·1 and 0·01. Two subsequent stages of dehydration are shown (fluids and restites 1 and 2). I2 marks the initial composition for the second stage and represents at the same time the restite R1 of the first dehydration stage with $D_B = 0{\cdot}1$. Calculations are based on the following parameters: H_2O content decreasing from 20 to 10 to 5 wt %; B concentration in initial rock 200 µg/g; $\delta^{11}B = +10‰$; $T = 100°C$ in first step and $T = 200°C$ in second step. The grey box represents the estimated composition of the blackwall-forming fluids.

significantly lower than those that could be in equilibrium with the tourmaline in the blackwalls from Syros. Although the model starts with an 'end-member' source (i.e. high B concentration and high $\delta^{11}B$ value), the $\delta^{11}B$ values of fluids released from this material strongly decrease after initial dehydration. As the highest B concentration and ^{11}B enrichment is found in low-temperature altered basalts, stored in clay minerals and pore water, the first release of fluid is likely to occur at very low temperatures during recrystallization below 150°C.

The release of high-pH fluids from the slab, as proposed by Manning (1998), would produce fluids with variable B concentrations, but uniform B isotope composition at any stage of dehydration. Their $\delta^{11}B$ value would be identical to that of the initial composition (+10‰ in the most extreme case). Therefore, it seems highly unlikely that the subducting slab is able to release fluids—acidic or basic—with $\delta^{11}B$ values of +28‰ or even +18‰ at depths of 25 km.

B budget of fluids migrating through the exhumation channel

As shown in the preceding section, the observed extreme enrichment of ^{11}B in the Syros blackwalls rules out any model that assumes tourmaline formation by direct precipitation from unmodified slab fluids. To solve this problem, one has to bear in mind that the exhuming mélange was probably separated from the subducting plate by several kilometres of ductile material (mica-, chlorite- and/or serpentine-rich rocks forming the 'exhumation channel' and the 'accretionary wedge'), rather than being in direct contact with it. Therefore, fluids escaping from the upper regions of the subducting slab would have had to migrate through a thick pile of rocks and must have been substantially modified before they reached the Syros melánge. The B isotopic evolution of the fluids will depend on their pH, as discussed above. Basic fluids, not fractionating the B isotopes, will simply approach the B isotopic composition of the rocks after travelling a certain distance. In contrast, acidic fluids will be successively enriched in ^{11}B and will evolve to progressively higher $\delta^{11}B$ values. The model presented below is an approach to predict the changes in both $\delta^{11}B$ and B concentration in an acidic fluid during its migration from the slab to the exhuming high-pressure blocks (i.e. the site of tourmaline formation).

The exact chemistry and mineralogy of the sequence of rocks composing the exhumation channel (hereafter called 'filter rock') cannot be determined precisely in the case of Syros. Although the matrix of the mélange may display the last portion of the fluid's pathway, its major part is probably not exposed. However, observations from other exhumed HP terrains may be used to describe the fluid-migration process in greater detail. HP mélanges in NE New Caledonia and in the Franciscan Complex, California, USA are interpreted to represent the subduction zone slab–mantle interface, an ideal site to study fluid–rock interaction processes above the slab (King *et al.*, 2003, 2004; Spandler *et al.*, 2003). The solubility and fluid mobility of various major and trace elements have been extracted from the mineralogical and bulk-rock chemical compositions. However, relatively little attention has been focused on the pH of such fluids. High-pH fluids have been found in serpentinites from the Mariana forearc seamounts (Savov *et al.*, 2005). Fluids released by hydrothermal vent systems located on serpentinites at the seafloor after serpentinization of peridotites also have very high pH (Kelley *et al.*, 2001), whereas fluids released after hydration of the basaltic oceanic crust are acidic, with pH between 2 and 5 (Humphris *et al.*, 1995). King *et al.* (2003, 2004) have investigated peridotite and serpentinite fragments in a mud-matrix mélange in the Franciscan Complex, and explained the observed B isotope evolution in these samples by a change of the fluids from high pH during initial serpentinization to low pH during later stages of silica metasomatism of the serpentinites. This demonstrates that the type and quantity of dissolved

components, as well as the pH of fluids migrating through the exhumation channel, are likely to be altered depending on the type of rocks they pass through. Initial hydration of ultramafic rocks will produce basic fluids, whereas the interaction with basaltic rocks will probably produce acidic fluids. Enduring flux of silica-rich fluids through serpentinites may also produce acidic fluids, as suggested by King *et al.* (2004). The blackwall-forming fluids on Syros probably interacted with serpentinites before they reached the HP blocks and may have varied in their pH during migration. Hence, they must have been acidic when they formed tourmaline. It can also be expected that conditions in the filter rock are not homogeneous and vary with time. The permeability, porosity, chemical and mineralogical composition of the filter rock, and temperature and fluid composition are probably affected by the fluid flux process. The B isotopic zonation of tourmaline in sample SY442, together with zoned omphacite, may be taken as evidence for changes of such a kind. In the model presented below, the input parameters are kept constant. However, calculations are performed with different input parameters to demonstrate their respective influence on the results.

In the model calculations, the fluid is assumed to be acidic along the entire flow path, as high-pH fluids in contact with sheet silicates will not fractionate the B isotopes and are, therefore, not able to explain the high δ^{11}B values of the tourmaline. The filter rock is assumed to be already saturated in H_2O prior to (further) fluid migration and will, thus, not remove H_2O from the fluid. H_2O-undersaturated filter rocks could also be included in the model and would result in a passive enrichment of B in the remaining fluid. Significant passive enrichment of B can occur only in cases where H_2O is quantitatively reduced by more than ~80%. As such an enrichment has no impact on the isotopic composition of the fluid, it was not considered in the model calculations presented below.

The model comprises a succession of steps of fluid–rock interaction with a consecutive change of input parameters for each step. The mass of filter rocks between the fluid source and the site of tourmaline formation is subdivided into a number of volumes and it is assumed that during migration through each rock volume complete equilibration between fluid and rock (with respect to B concentration and isotopic composition) is achieved. The resulting characteristics of the fluid generated through step n serve as initial parameters for step $n + 1$. Such a succession of fluid–rock interaction steps is, on the one hand, easy to calculate and allows for control of the impact of different parameters, and, on the other hand, is thought to reasonably represent the actual processes affecting the composition of the migrating fluid.

It is assumed that B in the filter rock is incorporated in minerals—serpentine, mica, amphiboles—in which it is tetrahedrally coordinated, whereas the fluids are probably acidic and, therefore, contain B in $B(OH)_3$ groups. B isotopic fractionation between filter rock and fluid was assumed to be determined by a change in coordination from trigonal in the fluid to tetrahedral in the rock and calculated using the formula given by Hervig *et al.* (2002) [equation (6)]. Other input parameters included in modelling the fluid–rock interaction process are: (1) the temperature of the rocks along the migration path; (2) the whole-rock–fluid partition coefficient for B (D_B); (3) B concentration and isotopic composition of the filter rock prior to the fluid flux; (4) B concentration and isotopic composition of the fluid at its starting point (i.e. when it leaves the dehydrating slab); (5) the fluid/rock ratio during interaction of migrating fluids with the filter rock. At first glance, one might think that the number of unknowns is too high for a meaningful model calculation, but a closer inspection reveals that the reasonable range of variation of some input parameters is rather restricted and the impact of others can be clearly evaluated.

The temperature of the high-pressure blocks was ~400°C at the time of tourmaline formation, as deduced above. They were located at a depth of ~25 km at that time. The subducting slab, releasing the hydrous B-bearing fluids, must have been at least at the same depth. However, the temperature in the upper part of the slab is lower than in the exhumation channel, as the exhuming rocks will transport heat advectively from greater depths towards the surface, whereas the slab is only slowly heated as it subducts. Isotherms are, therefore, bent upwards in the exhumation channel, but downwards in the slab. Temperatures during dehydration in the slab might, therefore, be lower than during rehydration in the overlying channel. Therefore, the filter model was calculated for a temperature of 400°C, but also for a lower temperature of 200°C, and for a fluid that is released at 200°C and continuously heated to 400°C as it reaches the HP blocks. The results for this heating path are located simply between the 200°C and the 400°C paths, and are not shown in the diagrams. The strong temperature dependence of B isotope fractionation results in a significant difference between the two calculations for 200°C and 400°C, as is displayed in Fig. 11.

Partition coefficients of B between hydrous fluid and rocks were discussed above. B is enriched in fluids relative to the rocks. The calculations for slab dehydration presented above were performed for D_B between 0·01 and 0·1. For the filter rock, possibly rich in sheet silicates, a partition coefficient of 0·01 might be too low, as sheet silicates (i.e. serpentine and white mica) readily incorporate B (e.g. Bonatti *et al.*, 1984; Domanik *et al.*,

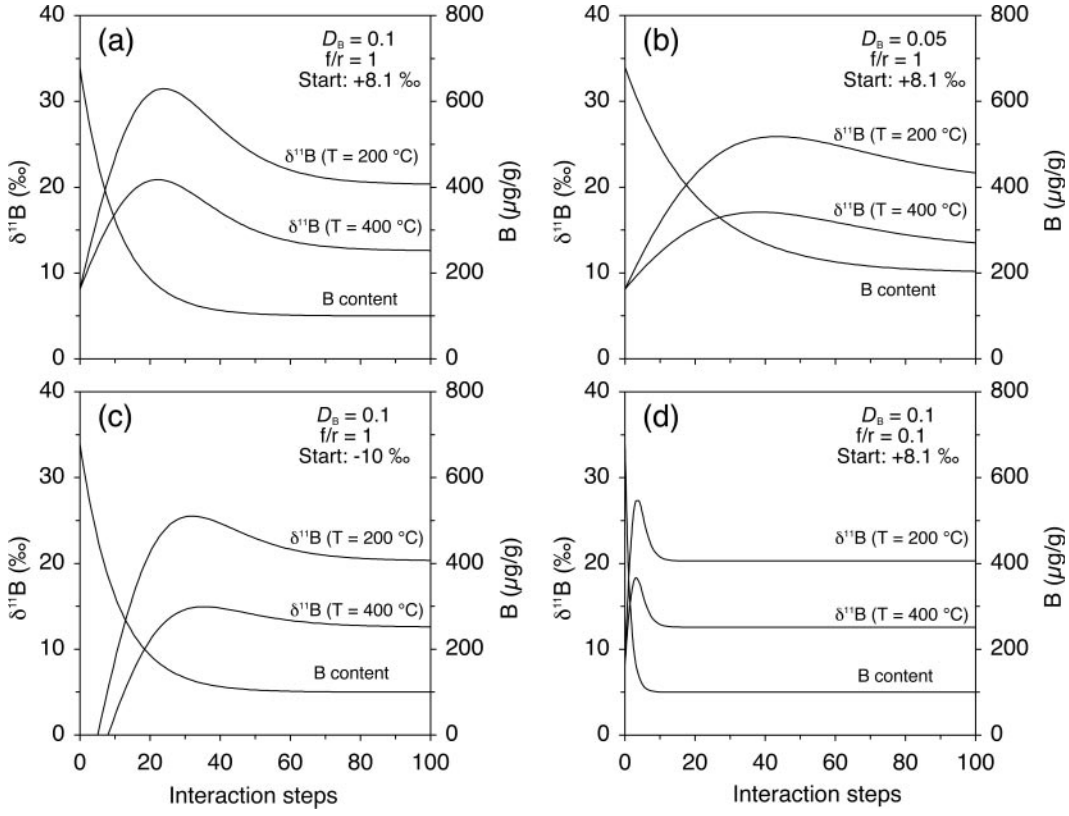

Fig. 11. Results of the model calculations on fluid–rock interaction with respect to $\delta^{11}B$ and B concentrations of evolving fluids for two temperatures (200°C and 400°C). Diagrams (a)–(d) are calculated for different input parameters: (a) whole-rock–fluid partition coefficient $D_B = 0{\cdot}1$, fluid/rock mass ratio of each step (f/r) = 1, $\delta^{11}B$ of initial fluid = +8·1‰; (b) $D_B = 0{\cdot}05$, f/r = 1, $\delta^{11}B$ = +8·1‰; (c) $D_B = 0{\cdot}1$, f/r = 1, $\delta^{11}B$ = –10·0‰; (d) $D_B = 0{\cdot}1$, f/r = 0·1, $\delta^{11}B$ = +8·1‰.

1993; Marschall, 2005). Therefore, calculations were performed for $D_B = 0{\cdot}1$ (Fig. 11a) and $D_B = 0{\cdot}05$ (Fig. 11b). A larger partition coefficient will result in a more intense and rapid change of both the $\delta^{11}B$ and B concentration of the fluid.

The B isotopic composition of the filter rock is not known, but its $\delta^{11}B$ value is assumed to be above that of the mantle (~–6‰), as serpentinites or other hydrated rocks are generated by interaction with hydrous fluids in the subduction zone. Such fluids generally show enrichment in ^{11}B, as was shown in the dehydration calculation above. To keep the results of the filter model more transparent, the calculation is performed with $\delta^{11}B = 0$‰ for the filter rock. More realistically, the values may range to much higher values, up to +15‰, as reported for serpentinites from forearc seamounts in the Marianas island arc by Benton *et al.* (2001). However, starting the calculation with a higher $\delta^{11}B$ value in the filter rock simply shifts the fluid $\delta^{11}B$ value in the same direction. (The extreme $\delta^{11}B$ value observed in sample SY442 may be explained by fluids that interacted with filter rocks with a higher initial $\delta^{11}B$ value.) The B concentration in the filter rock was assumed to be 10 μg/g, which is in the range of B concentrations of Syros serpentinites (5·5–11·3 μg/g) and mica-bearing blueschists (3·2–18·2 μg/g; Marschall, 2005). Significantly higher B concentrations in the filter rock lead to very rapid isotopic equilibration between fluid and filter rock. The system in this case is buffered by the filter.

The parameters for the fluid are taken from the dehydration model, described above. The B concentration (680 μg/g) and isotopic composition ($\delta^{11}B$ = +8·1‰) of the fluid are the values produced after the second dehydration step using a value of 0·1 for D_B. To estimate the impact of a completely different initial composition of the fluid, the calculation was also performed for $\delta^{11}B$ = –10·0‰ (Fig. 11c).

The incremental fluid/rock ratio is the parameter with the highest uncertainty and may also vary along the migration path of the fluid. Flow along discrete pathways ('veins') causes higher fluid/rock ratios than percolation through the rock along grain boundaries. Because of the lack of detailed information on the mechanisms of fluid transport and fluid/rock ratios, the calculations were performed for a fluid/rock ratio of unity (by mass).

The influence of this parameter on the results can be estimated from a second calculation for a value of 0·1, displayed in Fig. 11d.

Independent of the input parameters, the resulting concentrations and isotopic compositions of the fluids show a similar evolution. During the first steps, the B concentration of the fluid strongly decreases, while the $^{11}B/^{10}B$ ratio strongly increases to very high values. This peak in $\delta^{11}B$ is reached at a point where the B concentration of the fluid is already low and close to equilibrium with the unaffected filter rock. After the peak in isotopic composition, the $\delta^{11}B$ of the fluid decreases, approaching equilibrium with the unaffected filter rock. In the calculation with the standard parameters ($D_{B\ start} = 0{\cdot}1$; fluid/rock mass ratio = 1; $\delta^{11}B_{start} = +8{\cdot}1‰$), the fluid reaches a $\delta^{11}B$ of +31·4‰ for $T = 200°C$ and +20·7‰ for $T = 400°C$ after 25 steps (Fig. 11a). After ~70 steps, the B isotopic composition and B concentration of the fluid are close to equilibrium with the unaltered filter rock and any information on the initial composition is lost. During the first steps, the B concentration of the fluid is still high and the B isotopic composition of both rock and fluid is largely controlled by B from the fluid. Therefore, the $\delta^{11}B$ value of the fluid is steadily increasing. As soon as the B concentration of the fluid is low enough, B in the filter rock controls the system and the isotopic ratio of the fluid decreases towards the equilibrium value. For parameter values other than the standard ones, the peak of the curve is shifted to an earlier or later step and to a higher or lower $\delta^{11}B$ value. For a lower fluid/rock ratio of 0·1, the peak is at 18·3‰ (for 400°C) after the third step and the fluid values are indistinguishable from equilibrium after ~10 steps (Fig. 11b). For a lower partition coefficient of $D_B = 0{\cdot}05$, the peak is at 17·1‰ (for 400°C) after 40 steps, but reaches the equilibrium only after more than 100 steps (Fig. 11c). Even for a much lower B isotopic initial composition of –10‰, the fluid reaches a very high $\delta^{11}B$ value of +15·0‰ (for 400°C) after ~35 steps and a value indistinguishable from equilibrium after ~70 steps (Fig. 11d).

Although an exact quantification of fluid modification with respect to B concentration and isotopic composition is not possible, the model calculations presented above clearly show that the extraordinarily high $\delta^{11}B$ values observed in the blackwall tourmaline from Syros can indeed be generated by tourmaline precipitation from slab-derived fluids that were modified during migration through filter rocks in the exhumation channel. The low SiO_2 activity of the blackwall rocks, as deduced above, may be taken as evidence for interaction of the fluid with serpentinite on its way through the exhumation channel. Figure 12 displays the relationship between $\delta^{11}B$ and B concentration of the fluid, using $D_B = 0{\cdot}1$, fluid/rock mass ratio = 1, B_{start} = 680 μg/g and $\delta^{11}B_{start} = +8{\cdot}1‰$. The comparison with the estimated composition of the tourmaline-forming fluids from Syros shows that the modelled fluid composition reaches the Syros tourmaline field after 10–15 steps.

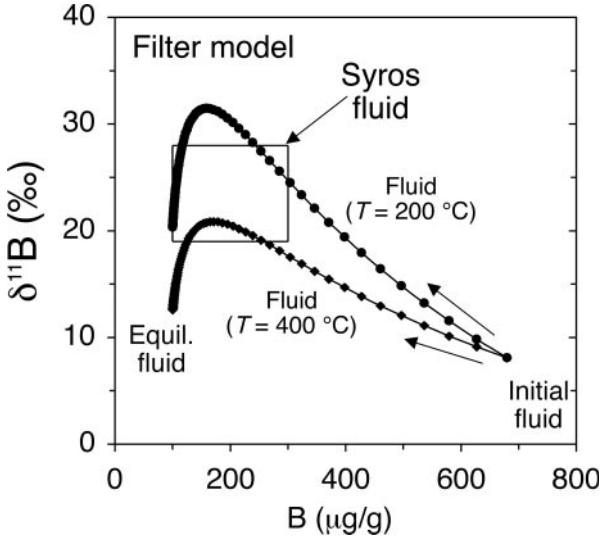

Fig. 12. $\delta^{11}B$ vs B concentration for fluids interacting with rocks during their ascent from the dehydrating slab through the exhumation channel. Parameters and results are equal to those of Fig. 11a: $D_B = 0{\cdot}1$, f/r = 1, $\delta^{11}B = +8{\cdot}1‰$. The box shows the estimated B concentration and B isotopic composition of tourmaline-forming fluids on Syros. Circles and diamonds show the evolution of the fluid for temperatures of 200°C and 400°C, respectively. Each point on the lines represents one step of fluid–rock interaction. Lines start on the right side (initial fluid) with parameters defined from the dehydration calculation (680 μg/g B; $\delta^{11}B = +8{\cdot}1‰$) and end on the left side at a point where fluid and filter rock are close to equilibrium (equil. fluid).

SUMMARY AND CONCLUSIONS

HP blocks enclosed in the mélange on the island of Syros are rimmed by blackwalls, which formed during exhumation of the HP mélange by influx of external hydrous fluids at ~0·6–0·75 GPa and 400–430°C. Tourmaline-bearing blackwall rocks are quartz-free and have SiO_2 activities of 0·4–0·5, generated during interaction of the rocks with low-SiO_2 fluids. Estimated B concentrations in the fluids are 100–300 μg/g, with isotopic compositions of +18 to +28‰ for $\delta^{11}B$.

H_2O and B in the fluids are likely to originate from the oceanic lithospheric slab that was still subducting as the Syros mélange was exhumed. The high $\delta^{11}B$ of tourmaline in the blackwalls cannot be explained by tourmaline formation from unmodified slab-derived fluids, because all known reservoirs in subducting slabs would produce a fluid with $\delta^{11}B$ below +10‰ at depths exceeding 20 km. However, interaction of acidic

slab-derived fluid with material composing the exhumation channel on its way from the dehydrating slab to the site of tourmaline formation in the blackwalls could produce exceptionally high $\delta^{11}B$ values in the fluids. In principle, this process is expected to take place within the subduction setting and is, therefore, favoured in this study to explain the ^{11}B enrichment in Syros tourmaline. The pH of hydrous fluid in equilibrium with different mineral parageneses at elevated *P* and *T* requires further investigation, as it has a significant impact on B isotope fractionation.

The calculated model demonstrates that fluids are effectively modified in both trace element and isotopic composition during their migration through the material overlying the subducting slab. Differences in B isotopic composition and concentration are blurred quickly and wiped out after short distances of migration, when the fluid approaches equilibrium with the rock composing the exhumation channel. Further investigation has to focus on the exact nature of fluid–rock interaction in accretionary wedges, in exhumation channels and at the slab–mantle interface, as these zones have a strong impact on the chemical and isotopic signatures that finally reach the surface within fluids and melts. The strong B isotope zonation in tourmaline of sample SY442 demonstrates that these interaction processes may rapidly change over short distances. The calculated model also suggests that the blackwall-forming fluids have not reached B isotopic equilibrium with the filter rock, but would have decreased in $\delta^{11}B$ during further migration, as is shown in Fig. 12.

The importance of B fixation, in particular of B with an isotopic composition affected by Earth surface processes, was emphasized by Nakano & Nakamura (2001), who investigated the B budget of metasedimentary rocks. They claimed that B is immobilized within the rocks as soon as it is fixed in tourmaline, which results in deep subduction of B into the mantle. Blackwall tourmaline as observed on Syros may have a similar impact on the B isotope cycle, as it has a large grain size (several centimetres), high abundance, and an exceptionally high $\delta^{11}B$ value, which is significantly different from the mantle value of ~–6‰. It is important to note that the blackwall tourmaline formed on the retrograde *P–T* path during exhumation of the rocks. One might, therefore, argue that blackwall tourmaline is not relevant for deep subduction processes. However, the formation of tourmaline at the contact between mafic or felsic HP blocks and their ultramafic matrix by fluids released during dehydration reactions in the subducting slab may also take place on the prograde path, wherever fluids are migrating through such contact zones (i.e. at the slab–mantle interface). If this is the case, the formation of blackwall tourmaline could have a significant impact on the geochemical cycle of B in subduction zones, as it fixes heavy B in large quantities within a highly stable mineral. Whether the tourmaline within the hydrated wedge material is dragged down with the slab or returned to the surface in an exhumation channel may vary with the overall tectonic setting of different subduction zones.

ACKNOWLEDGEMENTS

The authors would like to thank Hans-Peter Meyer and Stefan Prowatke for microprobe maintenance and for providing mineral formula calculation programs. This paper benefited from discussions with Stefan Prowatke, John Schumacher and Thomas Zack. Emily Lowe helped to improve the English style. Ilona Fin and Oliver Wienand are thanked for preparing high-quality thin sections for electron and ion microprobe investigations. This paper benefited from critical, encouraging and constructive reviews by Robbie King, Bill Leeman, Jeff Ryan and Jinnie Sisson, and from editorial handling by Marjorie Wilson. It resulted from the Dr. rer. nat. thesis of H.M. and was financially supported by the Deutsche Forschungsgemeinschaft (DFG, grants KA 1023/8-1 and AL 166/15-3), which is gratefully acknowledged.

REFERENCES

Ai, Y. (1994). A revision of the garnet–clinopyroxene Fe^{2+}–Mg exchange geothermometer. *Contributions to Mineralogy and Petrology* **115**, 467–473.

Altherr, R., Topuz, G., Marschall, H., Zack, T. & Ludwig, T. (2004). Evolution of a tourmaline-bearing lawsonite eclogite from Elekdag area (Central Pontides, N Turkey): evidence for infiltration of slab-derived B-rich fluids during exhumation. *Contributions to Mineralogy and Petrology* **148**, 409–425.

Ballhaus, C. & Schumacher, J. C. (1995). Stratigraphy, deformation and high-pressure metamorphism of the island of Syros (Cyclades, Greece). *Bochumer Geologische und Geotechnische Arbeiten* **44**, 13–16.

Barth, S. (1998). $^{11}B/^{10}B$ variations of dissolved boron in a freshwater–seawater mixing plume (Elbe Estuary, North Sea). *Marine Chemistry* **62**, 1–14.

Bebout, G. E. (1996). Volatile transfer and recycling at convergent margins: mass-balance and insights from high *P/T* metamorphic rocks (overview). In: Bebout, G. E., Scholl, D. W., Kirby, S. H. & Platt, J. P. (eds) *Subduction Top to Bottom. Geophysical Monograph, American Geophysical Union* **96**, 179–194.

Bebout, G. E. & Barton, M. D. (2002). Tectonic and metasomatic mixing in a high-*T*, subduction-zone mélange—insights into the geochemical evolution of the slab–mantle interface. *Chemical Geology* **187**, 79–106.

Bebout, G. E. & Nakamura, E. (2003). Record in metamorphic tourmaline of subduction-zone devolatilization and boron cycling. *Geology* **31**, 407–410.

Bebout, G. E., Ryan, J. G., Leeman, W. P. & Bebout, A. E. (1999). Fractionation of trace elements by subduction-zone metamorphism—effect of convergent-margin thermal evolution. *Earth and Planetary Science Letters* **171**, 63–81.

Benton, L. D., Ryan, J. G. & Tera, F. (2001). Boron isotope systematics of slab fluids as inferred from a serpentine seamount, Mariana forearc. *Earth and Planetary Science Letters* **187**, 273–282.

Bonatti, E., Lawrence, J. R. & Morandi, N. (1984). Serpentinization of oceanic peridotites: temperature dependence of mineralogy and boron content. *Earth and Planetary Science Letters* **70**, 88–94.

Bonneau, M., Geyssant, J., Kienast, J. R., Lepvrier, C. & Maluski, H. (1980). Tectonique et métamorphisme haute pression d'âge éocène dans les Hellénides: exemple de l'île de Syros (Cyclades, Grèce). *Comptes Rendus de l'Académie des Sciences, Série D* **291**, 171–174.

Brady, J. B., Able, L. M., Cheney, J. T., Sperry, A. J. & Schumacher, J. C. (2001). Prograde lawsonite pseudomorphs in blueschists from Syros, Greece. *Geological Society of America, Abstracts with Programs* **33**, 250–251.

Brady, J. B., Markley, M. J., Schumacher, J. C., Cheney, J. T. & Bianciardi, G. A. (2004). Aragonite pseudomorphs in high-pressure marbles of Syros, Greece. *Journal of Structural Geology* **26**, 3–9.

Brenan, J. M., Neroda, E., Lindstrom, C. C., Shaw, H. F., Ryerson, F. J. & Phinney, D. L. (1998*a*). Behavior of boron, beryllium and lithium during melting and crystallization: constraints from mineral–melt partitioning experiments. *Geochimica et Cosmochimica Acta* **62**, 2129–2141.

Brenan, J. M., Ryerson, F. J. & Shaw, H. F. (1998*b*). The role of aqueous fluids in the slab-to-mantle transfer of boron, beryllium, and lithium during subduction: experiments and models. *Geochimica et Cosmochimica Acta* **62**, 3337–3347.

Bröcker, M. & Enders, M. (2001). Unusual bulk-rock compositions in eclogite-facies rocks from Syros and Tinos (Cyclades, Greece): implications for U–Pb zircon geochronology. *Chemical Geology* **175**, 581–603.

Carson, C. J., Clarke, G. L. & Powell, R. (2000). Hydration of eclogite from the Pam Peninsula, New Caledonia. *Journal of Metamorphic Geology* **18**, 79–90.

Catanzaro, F. J., Champion, C. E., Garner, E. L., Marinenko, G., Sappenfield, K. M. & Shields, W. R. (1970). Boric acid: isotopic and assay standard reference materials. *National Bureau of Standards (US) Special Publications* **260**, 1–70.

Chaussidon, M. & Jambon, A. (1994). Boron content and isotopic composition of oceanic basalts: geochemical and cosmochemical implications. *Earth and Planetary Science Letters* **121**, 277–291.

Deyhle, A. & Kopf, A. (2002). Strong B enrichment and anomalous δ^{11}B in pore fluids from the Japan trench forearc. *Marine Geology* **183**, 1–15.

Dingwell, D. B., Pichavant, M. & Holtz, F. (2002). Experimental studies of boron in granitic melts. In: Grew, E. S. & Anovitz, L. M. (eds) *Boron: Mineralogy, Petrology and Geochemistry. Mineralogical Society of America, Reviews in Mineralogy* **33**, 331–385.

Dixon, J. E. (1968). The metamorphic rocks of Syros, Greece. Ph.D. thesis. St. John's College, Cambridge.

Dixon, J. E. & Ridley, J. (1987). Syros. In: Helgeson, H. C. (ed.) *Chemical Transport in Metasomatic Processes. NATO ASI Series C, Mathematical and Physical Sciences* **218**, 489–501.

Domanik, K. J., Hervig, R. L. & Peacock, S. M. (1993). Beryllium and boron in subduction zone minerals: an ion microprobe study. *Geochimica et Cosmochimica Acta* **57**, 4997–5010.

Dürr, S., Altherr, R., Keller, J., Okrusch, M. & Seidel, E. (1978). The median Aegean crystalline belt: stratigraphy, structure, metamorphism, magmatism. In: Closs, H., Roeder, D. H. & Schmidt, K. (eds) *Alps, Apennines, Hellenides. Inter-Union Commission on Geodynamics, Scientific Reports* **38**, 455–477.

Dyar, M. D., Taylor, M. E., Lutz, T. M., Francis, C. A., Guidotti, C. V. & Wise, M. (1998). Inclusive chemical characterization of tourmaline: Mössbauer study of Fe valence and site occupancy. *American Mineralogist* **83**, 848–864.

Dyar, M. D., Wiedenbeck, M., Robertson, D., Cross, L. R., Delaney, J. S., Ferguson, K., Francis, C. A., Grew, E. S., Guidotti, C. V., Hervig, R. L., Hughes, J. M., Husler, J., Leeman, W., McGuire, A. V., Rhede, D., Rothe, H., Paul, R. L., Richards, I. & Yates, M. (2001). Reference minerals for the microanalysis of light elements. *Geostandards Newsletter* **25**, 441–463.

Engi, M., Berger, A. & Roselle, G. T. (2001). Role of the tectonic accretion channel in collisional orogeny. *Geology* **29**, 1143–1146.

Ernst, W. G. (2001). Subduction, ultrahigh-pressure metamorphism, and regurgitation of buoyant crustal slices; implications for arcs and continental growth. *Physics of the Earth and Planetary Interiors* **127**, 253–275.

Evans, B. W., Trommsdorff, V. & Richter, W. (1979). Petrology of an eclogite–metarodingite suite at Cima di Gagnone, Ticino, Switzerland. *American Mineralogist* **64**, 15–31.

Fitzherbert, J. A., Clarke, G. L., Marmo, B. & Powell, R. (2004). The origin and *P–T* evolution of peridotites and serpentinites of NE New Caledonia: prograde interaction between continental margin and the mantle wedge. *Journal of Metamorphic Geology* **22**, 327–344.

Gerya, T. V., Stoeckhert, B. & Perchuk, A. L. (2002). Exhumation of high-pressure metamorphic rocks in a subduction channel; a numerical simulation. *Tectonics* **21**, 6–19.

Guillot, S., Hattori, K. H., de Sigoyer, J., Nägler, T. & Auzende, A.-L. (2001). Evidence of hydration of the mantle wedge and its role in the exhumation of eclogites. *Earth and Planetary Science Letters* **193**, 115–127.

Harder, H. (1970). . Boron content of sediments as a tool in facies analysis. *Sedimentary Geology* **4**, 153–175.

Hawthorne, F. C. & Henry, D. J. (1999). Classification of the minerals of the tourmaline group. *European Journal of Mineralogy* **11**, 201–215.

Hecht, J. (1984). *Geological map of Greece 1:50 000, Syros island*. Athens: Institute of Geology and Mineral Exploration.

Heinrich, W., Wunder, B., Romer, R. L., Meixner, A. & Wirth, R. (2003). B-isotope-distribution between boro-muscovite and fluid: first results of an experimental study. *Berichte der Deutschen Mineralogischen Gesellschaft, Beiheft 1 zu European Journal of Mineralogy* **15**, 79.

Hemming, N. G. & Hanson, G. N. (1992). Boron isotopic composition and concentration in modern marine carbonates. *Geochimica et Cosmochimica Acta* **56**, 537–543.

Hervig, R. L., Moore, G. M., Williams, L. B., Peacock, S. M., Holloway, J. R. & Roggensack, K. (2002). Isotopic and elemental partitioning of boron between hydrous fluid and silicate melt. *American Mineralogist* **87**, 769–774.

Humphris, S. E., Zierenberg, R. A., Mullineau, L. S. & Thomson, R. E. (eds) *Seafloor Hydrothermal Systems: Physical, Chemical, Biological, and Geological Interactions. Geophysical Monograph, American Geophysical Union* **91**.

Ishikawa, T. & Nakamura, E. (1994). Origin of the slab component in arc lavas from across-arc variation of B and Pb isotopes. *Nature* **370**, 205–208.

Ishikawa, T. & Tera, F. (1997). Source, composition and distribution of the fluid in the Kurile mantle wedge: constraints from across-arc variations of B/Nb and B isotopes. *Earth and Planetary Science Letters* **152**, 123–138.

Ishikawa, T., Tera, F. & Nakazawa, T. (2001). Boron isotope and trace element systematics of the three volcanic zones in the Kamchatka arc. *Geochimica et Cosmochimica Acta* **65**, 4523–4537.

Jolivet, L., Faccenna, C., Goffé, B., Burov, E. & Agard, P. (2003). Subduction tectonics and exhumation of high-pressure metamorphic rocks in the Mediterranean orogens. *American Journal of Science* **303**, 353–409.

Kalt, A., Schreyer, W., Ludwig, T., Prowatke, S., Bernhardt, H.-J. & Ertl, A. (2001). Complete solid solution between magnesian schorl and lithian excess-boron olenite in a pegmatite from the Koralpe (eastern Alps, Austria). *European Journal of Mineralogy* **13**, 1191–1205.

Keiter, M., Piepjohn, K., Ballhaus, C., Bode, M. & Lagos, M. (2004). Structural development of high-pressure metamorphic rocks on Syros island (Cyclades, Greece). *Journal of Structural Geology* **26**, 1433–1445.

Kelley, D. S., Karson, J. A., Blackman, D. K., Früh-Green, G. L., Butterfield, D. A., Lilley, M. D., Olson, E. J., Schrenk, M. O., Roe, K. K., Lebon, G. T. & Rivizzigno, P. & the AT 3-60 Shipboard Party (2001). An off-axis hydrothermal vent field near the Mid-Atlantic Ridge at 30°N. *Nature* **412**, 145–149.

King, R. L., Kohn, M. J. & Eiler, J. M. (2003). Constraints on the petrologic structure of the subduction zone slab–mantle interface from Franciscan Complex exotic ultramafic blocks. *Geological Society of America Bulletin* **115**, 1097–1109.

King, R. L., Savov, I. P., Bebout, G. E., Tonarini, S. & Ryan, J. G. (2004). Metasomatic mechanisms for fractionation of slab-derived B isotope signatures within the mantle wedge: evidence from HP-metasomatized peridotites. *EOS Transactions, American Geophysical Union, Fall Meeting Supplement* **85**, V11C-03.

Kopf, A. & Deyhle, A. (2002). Back to the roots; boron geochemistry of mud volcanoes and its implications for mobilization depth and global B cycling. *Chemical Geology* **192**, 195–210.

Krogh, Ravna, E. (2000). The garnet–clinopyroxene Fe^{2+}–Mg geothermometer: an update calibration. *Journal of Metamorphic Geology* **18**, 211–219.

Leeman, W. P. (1996). Boron and other fluid-mobile elements in volcanic arc lavas: implications for subduction processes. In: Bebout, G. E., Scholl, D. W., Kirby, S. H. & Platt, J. P. (eds) *Subduction Top to Bottom. Geophysical Monograph, American Geophysical Union* **96**, 269–276.

Leeman, W. P. & Sisson, V. B. (2002). Geochemistry of boron and its implications for crustal and mantle processes. In: Grew, E. S. & Anovitz, L. M. (eds) *Boron: Mineralogy, Petrology and Geochemistry. Mineralogical Society of America, Reviews in Mineralogy* **33**, 645–708.

Leeman, W. P. & Tonarini, S. (2001). Boron isotopic analysis of proposed borosilicate mineral reference samples. *Geostandards Newsletter* **25**, 399–403.

Liou, J. G., Hacker, B. R. & Zhang, R. Y. (1997). Into the forbidden zone. *Science* **287**, 1215–1216.

Manning, C. E. (1998). Fluid composition at the blueschist–eclogite transition in the model system Na_2O–MgO–Al_2O_3–SiO_2–H_2O–HCl. *Schweizer Mineralogische und Petrographische Mitteilungen* **78**, 225–242.

Marschall, H. R. (2005). Lithium, beryllium, and boron in high-pressure metamorphic rocks from Syros (Greece). , Dr. rer. nat. thesis, Universität Heidelberg. http://www.ub.uni-heidelberg.de/archiv/5634.

Marschall, H. R. & Ludwig, T. (2004). The low-boron contest: minimising surface contamination and analysing boron concentrations at the ng/g-level by secondary ion mass spectrometry. *Mineralogy and Petrology* **81**, 265–278.

Marschall, H. R., Ertl, A., Hughes, J. M. & McCammon, C. (2004). Metamorphic Na- and OH-rich disordered dravite with tetrahedral boron, associated with omphacite, from Syros, Greece: chemistry and structure. *European Journal of Mineralogy* **16**, 817–823.

McDonough, W. F. & Sun, S.-S. (1995). The composition of the Earth. *Chemical Geology* **120**, 223–253.

Moran, A. E., Sisson, V. B. & Leeman, W. P. (1992). Boron depletion during progressive metamorphism: implications for subduction processes. *Earth and Planetary Science Letters* **111**, 331–349.

Morgan, G. B.,IV & London, D. (1989). Experimental reactions of amphibolite with boron-bearing aqueous fluids at 200 MPa: implications for tourmaline stability and partial melting in mafic rocks. *Contributions to Mineralogy and Petrology* **102**, 281–297.

Morimoto, N., Fabries, J., Ferguson, A. K., Ginzburg, I. V., Ross, M., Seifert, F. A., Zussman, J., Aoki, K. & Gottardi, G. (1988). Nomenclature of pyroxenes. . *American Mineralogist* **73**, 1123–1133.

Nakano, T. & Nakamura, E. (2001). Boron isotope geochemistry of metasedimentary rocks and tourmalines in a subduction zone metamorphic suite. *Physics of the Earth and Planetary Interiors* **127**, 233–252.

Och, D. J., Leitch, E. C., Caprarelli, G. & Watanabe, T. (2003). Blueschist and eclogite in tectonic melange, Port Macquarie, New South Wales, Australia. *Mineralogical Magazine* **67**, 609–624.

Okrusch, M. & Bröcker, M. (1990). Eclogites associated with high-grade blueschists in the Cyclades archipelago, Greece: a review. *European Journal of Mineralogy* **2**, 451–478.

Palmer, M. R. & Swihart, G. H. (2002). Boron isotope geochemistry: an overview. In: Grew, E. S. & Anovitz, L. M. (eds) *Boron: Mineralogy, Petrology and Geochemistry. Mineralogical Society of America, Reviews in Mineralogy* **33**, 709–744.

Palmer, M. R., London, D., Morgan, G. B.,IV & Babb, H. (1992). Experimental determination of fractionation of $^{11}B/^{10}B$ between tourmaline and aqueous vapor: a temperature- and pressure-dependent isotopic system. *Chemical Geology* **101**, 123–129.

Peacock, S. M. (1990). Fluid processes in subduction zones. *Science* **248**, 329–337.

Peacock, S. M. & Hervig, R. L. (1999). Boron isotopic composition of subduction-zone metamorphic rocks. *Chemical Geology* **160**, 281–290.

Pearce, N. J. G., Perkins, W. T., Westgate, J. A., Gorton, M. P., Jackson, S. E., Neal, C. R. & Chenery, S. P. (1997). A compilation of new and published major and trace element data for NIST SRM 610 and NIST SRM 612 glass reference materials. *Geostandards Newsletter* **21**, 115–144.

Pouchou, J. L. & Pichoir, F. (1984). A new model for quantitative analyses. I. Application to the analysis of homogeneous samples. *La Recherche Aérospatiale* **3**, 13–38.

Pouchou, J. L. & Pichoir, F. (1985). 'PAP' (φ–ρ–Z) correction procedure for improved quantitative microanalysis. In: Armstrong, J. T. (ed.) *Microbeam Analysis*. San Francisco, CA: San Francisco Press, pp. 104–106.

Powell, R. & Holland, T. J. B. (1988). An internally consistent dataset with uncertainties and correlations; 3, Applications to geobarometry, worked examples and a computer program. *Journal of Metamorphic Geology* **6**, 173–204.

Powell, R., Holland, T. J. B. & Worley, B. (1998). Calculating phase diagrams involving solid solutions via non-linear equations, with examples using THERMOCALC. *Journal of Metamorphic Geology* **16**, 577–588.

Putlitz, B., Cosca, M. A. & Schumacher, J. C. (2005). Prograde mica $^{40}Ar/^{39}Ar$ growth ages recorded in high pressure rocks (Syros, Cyclades, Greece). *Chemical Geology* **214**, 79–98.

Rice, J. M., Evans, B. W. & Trommsdorff, V. (1974). Widespread occurrence of magnesio-cummingtonite, Cima di Gagnone, Ticino, Switzerland. *Contributions to Mineralogy and Petrology* **43**, 245–251.

Ridley, J. (1982). Arcuate lineation trends in a deep level, ductile thrust belt, Syros, Greece. *Tectonophysics* **88**, 347–360.

Ridley, J. (1984). Evidence for temperature-dependent 'blueschist' to 'eclogite' transformation in high-pressure metamorphism of metabasic rocks. *Journal of Petrology* **25**, 852–870.

Ridley, J. (1986). Parallel stretching lineations and fold axes oblique to a shear displacement direction—a model and observations. *Journal of Structural Geology* **8**, 647–653.

Ring, U. & Fleischmann, T. (2002). The weak and superfast Cretan detachment, Greece: exhumation at subduction rates in extruding wedges. *Journal of the Geological Society, London* **159**, 225–228.

Ring, U., Thomson, S. N. & Bröcker, M. (2003). Fast extension but little exhumation: the Vari detachment in the Cyclades, Greece. *Geological Magazine* **140**, 245–252.

Roselle, G. T. & Engi, M. (2002). Ultra high pressure (UHP) terrains; lessons from thermal modeling. *American Journal of Science* **302**, 410–441.

Rosenbaum, G., Avigad, D. & Sánchez-Gómez, M. (2002). Coaxial flattening at deep levels of orogenic belts: evidence from blueschists and eclogites on Syros and Sifnos (Cyclades, Greece). *Journal of Structural Geology* **24**, 1451–1462.

Rubatto, D. & Hermann, J. (2001). Exhumation as fast as subduction? *Geology* **29**, 3–6.

Ryan, J. G. & Langmuir, C. H. (1993). The systematics of boron abundances in young volcanic rocks. *Geochimica et Cosmochimica Acta* **57**, 1489–1498.

Sanchez-Valle, C., Reynard, B., Daniel, I., Lecuyer, C., Martinez, I. & Chervin, J. C. (2005). Boron isotope fractionation between minerals and fluids: new insights from *in situ* high pressure–high temperature vibrational spectroscopic data. *Geochimica et Cosmochimica Acta* **69**, 4301–4313.

Savov, I. P., Guggino, S., Ryan, J. G., Fryer, P. & Mottl, M. J. (2005). Geochemistry of serpentinite mud and metamorphic rocks from the Mariana forearc, ODP sites 1200 and 778–779, South Chamorro and Conical seamounts. In: Shinora, M., Salisbury, M. H. & Richter, C. (eds), *Proceedings of the Ocean Drilling Program, Scientific Results, 195* College Station, TX: Ocean Drilling Program, pp. 1–49.

Scambelluri, M., Müntener, O., Ottolini, L., Pettke, T. T. & Vanucci, R. (2004). The fate of B, Cl and Li in subducted oceanic mantle and in the antigorite breakdown fluids. *Earth and Planetary Science Letters* **222**, 217–234.

Schmidt, C., Thomas, R. & Heinrich, W. (2005). Boron speciation in aqueous fluids at 22 to 600°C and 0·1 to 2 GPa. *Geochimica et Cosmochimica Acta* **69**, 275–281.

Schmidt, M. W. & Poli, S. (1998). Experimentally based water budgets for dehydrating slabs and consequences for arc magma generation. *Earth and Planetary Science Letters* **163**, 361–379.

Schumacher, J. C. (1997). The estimation of ferric iron in electron analysis of amphiboles. *European Journal of Mineralogy* **9**, 643–651.

Seck, H. A., Kötz, J., Okrusch, M., Seidel, E. & Stosch, H.-G. (1996). Geochemistry of a meta-ophiolite suite: an association of metagabbros, eclogites and glaucophanites on the island of Syros, Greece. *European Journal of Mineralogy* **8**, 607–623.

Shreve, R. L. & Cloos, M. (1986). Dynamics of sediment subduction, mélange formation, and prism accretion. *Journal of Geophysical Research* **91**, 10229–10245.

Sorensen, S. S. & Grossman, J. N. (1989). Enrichment of trace elements in garnet amphibolites from a paleo-subduction zone: Catalina Schist, southern California. *Geochimica et Cosmochimica Acta* **53**, 3155–3177.

Spandler, C., Hermann, J., Arculus, R. & Mavrogenes, J. (2003). Redistribution of trace elements during prograde metamorphism from lawsonite blueschist to eclogite facies; implications for deep subduction-zone processes. *Contributions to Mineralogy and Petrology* **146**, 205–222.

Taylor, S. R. & McLennan, S. M. (1995). The geochemical evolution of the continental crust. *Reviews in Geophysics* **33**, 241–265.

Tonarini, S., Pennisi, M. & Leeman, W. P. (1997). Precise boron isotopic analysis of silicate (rock) samples using alkali carbonate fusion and ion-exchange separation. *Chemical Geology* **142**, 129–137.

Tonarini, S., Dini, A., Pezzotta, F. & Leeman, W. P. (1998). Boron isotopic compositions of zoned (schorl–elbaite) tourmaline, Mt. Capanne Li–Cs pegmatites, Elba (Italy). *European Journal of Mineralogy* **10**, 941–952.

Trotet, F., Jolivet, L. & Vidal, O. (2001a). Tectono-metamorphic evolution of Syros and Sifnos islands (Cyclades, Greece). *Tectonophysics* **338**, 179–206.

Trotet, F., Vidal, O. & Jolivet, L. (2001b). Exhumation of Syros and Sifnos metamorphic rocks (Cyclades, Greece). New constraints on the *P–T* paths. *European Journal of Mineralogy* **13**, 901–920.

Ulmer, P. & Trommsdorff, V. (1995). Serpentinite stability to mantle depths and subduction-related magmatism. *Science* **268**, 858–861.

Weisbrod, A., Polak, C. & Roy, D. (1986). Experimental study of tourmaline solubility in the system Na–Mg–Al–Si–B–O–H. Applications to the boron content of natural hydrothermal fluids and tourmalinization processes. *Experimental Mineralogy and Geochemistry International Symposium, Nancy, Abstracts*, 140.

Werding, G. & Schreyer, W. (2002). Experimental studies on borosilicates and selected borates. In: Grew, E. S. & Anovitz, L. M. (eds) *Boron: Mineralogy, Petrology and Geochemistry. Mineralogical Society of America. Reviews in Mineralogy* **33**, 117–163.

Williams, L. B., Hervig, R. L., Holloway, J. R. & Hutcheon, I. (2001). B isotope geochemistry during diagenesis. Part I. Experimental determination of fractionation during illitization of smectite. *Geochimica et Cosmochimica Acta* **65**, 1769–1782.

Wunder, B. & Schreyer, W. (1997). Antigorite: high-pressure stability in the system MgO–SiO_2–H_2O (MSH). *Lithos* **41**, 213–227.

Wunder, B., Meixner, A., Romer, R. L. & Heinrich, W. (2004). The geochemical cycle of boron: experiments on boron isotope patitioning between micas and fluids. *Geochimica et Cosmochimica Acta, Supplement* **68**, A51.

You, C.-F., Castillo, P. R., Gieskes, J. M., Chan, L. H. & Spivack, A. J. (1996a). Trace element behavior in hydrothermal experiments: implications for fluid processes at shallow depth in subduction zones. *Earth and Planetary Science Letters* **140**, 41–52.

You, C.-F., Spivack, A. J., Gieskes, J. M., Martin, J. B. & Davisson, M. L. (1996b). Boron contents and isotopic compositions in pore waters: a new approach to determine temperature induced artifacts—geochemical implications. *Marine Geology* **129**, 351–361.

APPENDIX: EQUATIONS USED FOR MODELLING

Boron concentrations in rocks and fluids during dehydration

For the calculation of light element concentrations in rocks and released fluids in the models, the following equation was used:

$$c_{\mathrm{B}}^{\mathrm{f}} = \frac{c_{\mathrm{B}}^{\mathrm{r}_{n-1}}}{(D_n - 1)(m_{\mathrm{r}_n}/m_{\mathrm{r}_{n-1}}) + 1} \qquad (7)$$

where $c_{\mathrm{B}}^{\mathrm{f}}$ is the concentration of B in the fluid, $c_{\mathrm{B}}^{\mathrm{r}_{n-1}}$ is the concentration of B in the rock before dehydration step n, D_n is the partition coefficient between dehydrated rock at step n and fluid, $m_{\mathrm{r}_{n-1}}$ is the mass of the rock before dehydration step n, and m_{r_n} is the mass of the rock after dehydration step n.

The following definitions are used: m_{f_n} is the mass of fluid released during dehydration step n, $c_{\mathrm{B}}^{\mathrm{r}_n}$ is the

concentration of B in the rock after dehydration step n, $m_B^{r_{n-1}}$ is the mass of B in the rock before dehydration step n, $m_B^{r_n}$ is the mass of B in the rock after dehydration step n, and $m_B^{f_n}$ is the mass of B in the fluid released during dehydration step n.

Equation (7) is derived from:

(1) mass balance between the masses of fluid and rock before and after dehydration

$$m_{r_{n-1}} = m_{r_n} + m_{f_n} \tag{8}$$

(2) mass balance between the masses of B in fluid and rock before and after dehydration

$$m_B^{r_{n-1}} = m_B^{r_n} + m_B^{f_n} \tag{9}$$

(3) the definition of the partition coefficient

$$D_n = \frac{c_B^{r_n}}{c_B^{f}} \tag{10}$$

(4) the definition of the concentration of B in rocks and fluid

$$c_B^{r_n} = \frac{m_B^{r_n}}{m_{r_n}} \tag{11}$$

$$c_B^{r_{n-1}} = \frac{m_B^{r_{n-1}}}{m_{r_{n-1}}} \Leftrightarrow m_B^{r_{n-1}} = c_B^{r_{n-1}} \cdot m_{r_{n-1}} \tag{12}$$

and

$$c_B^{f_n} = \frac{m_B^{f_n}}{m_{f_n}} \Leftrightarrow m_B^{f_n} = c_B^{f_n} \cdot m_{f_n}. \tag{13}$$

The combination of equations (10), (11) and (13) results in

$$D_n = \frac{m_B^{r_n}}{m_B^{f_n}} \cdot \frac{m_{f_n}}{m_{r_n}}. \tag{14}$$

Combining this equation with equation (8) and solving it for $m_B^{f_n}$ results in

$$m_B^{f_n} = \frac{m_B^{r_{n-1}}}{D_n(m_{r_{n-1}}/m_{f_n}) + 1}. \tag{15}$$

Replacing the mass of element i in the fluid by its concentration, using equation (13) results in

$$c_B^{f} = \frac{m_B^{r_{n-1}}}{D_n m_{r_n} m_{f_n}}. \tag{16}$$

Replacing the mass of B in the rock by its concentration, using equation (12), and the mass of the fluid by the mass difference between the rock before and after dehydration [equation (8)] results in equation (7).

Isotope fractionation during dehydration

For the calculation of B isotopic ratios of fluids and rocks during dehydration, the mass balance calculations were extended by using:

(1) mass balance between the two isotopes of B in fluid and rock

$$m_{10}^{f_n} + m_{11}^{f_n} = m_B^{f_n} \tag{17}$$

$$m_{10}^{r_n} + m_{11}^{r_n} = m_B^{r_n} \tag{18}$$

(2) mass balance of the B isotopes in fluid and rock before and after dehydration

$$m_{10}^{r_n} + m_{10}^{f_n} = m_{10}^{r_{n-1}} \tag{19}$$

$$m_{11}^{r_n} + m_{11}^{f_n} = m_{11}^{r_{n-1}} \tag{20}$$

(3) the definition of $\delta^{11}B$, for both fluid and rock

$$\delta^{11}B_{f_n} = \left[\frac{(m_{11}^{f_n}/m_{10}^{f_n})}{(m_{11}^{Std}/m_{10}^{Std})} - 1\right] \cdot 1000 \tag{21}$$

$$\delta^{11}B_{r_n} = \left[\frac{(m_{11}^{r_n}/m_{10}^{r_n})}{(m_{11}^{Std}/m_{10}^{Std})} - 1\right] \cdot 1000 \tag{22}$$

(4) the definition of the isotopic fractionation between fluid and rock

$$\Delta^{11}B = \delta^{11}B_{f_n} - \delta^{11}B_{r_n} \tag{23}$$

where $m_{10}^{f_n}$ is the calculated mass of ^{10}B in the fluid at dehydration step n, $m_{11}^{f_n}$ is the mass of ^{11}B calculated in the fluid at dehydration step n, $m_{10}^{r_n}$ is the mass of ^{10}B in the rock after dehydration step n, $m_{11}^{r_n}$ is the mass of ^{11}B in the rock after dehydration step n, $m_{10}^{r_{n-1}}$ is the mass of ^{10}B in the rock before dehydration step n, $m_{11}^{r_{n-1}}$ is the mass of ^{11}B in the rock before dehydration step n, $m_{11}^{Std}/m_{10}^{Std}$ is the B isotope ratio in standard material SRM 951, $\delta^{11}B_{f_n}$ is the B isotope ratio of the fluid released at dehydration step n, in δ-notation relative to SRM 951, $\delta^{11}B_{r_n}$ is the B isotope ratio of the rock after dehydration step n, in δ-notation relative to SRM 951, and $\Delta^{11}B$ is the difference in the B isotopic ratio (in δ-notation) between rock and fluid.

The masses of boron in fluid ($m_B^{f_n}$) and rock ($m_B^{r_n}$) are calculated as indicated above. The B isotope ratio and concentrations ($m_{10}^{r_{n-1}}$,$m_{11}^{r_{n-1}}$) in the rock before dehydration are known. The B isotopic fractionation is temperature dependent and is calculated using the formula given by Hervig *et al.* (2002). The following mass balance calculation is used to determine the $\delta^{11}B$ values of the rock after dehydration step n and of the released fluid. Values for standard reference material SRM 951 are taken from Catanzaro *et al.* (1970).

Combining equations (21), (22) and (23) results in

$$\frac{m_{11}^{f_n}}{m_{10}^{f_n}} - \frac{m_{11}^{r_n}}{m_{10}^{r_n}} = \frac{\Delta^{11}B}{1000} \cdot \frac{m_{11}^{Std}}{m_{10}^{Std}}. \quad (24)$$

Combining equation (24) with equations (19) and (20) results in

$$\frac{m_{11}^{r_{n-1}} - m_{11}^{r_n}}{m_{10}^{r_{n-1}} - m_{10}^{r_n}} - \frac{m_{11}^{r_n}}{m_{10}^{r_n}} = \frac{\Delta^{11}B}{1000} \cdot \frac{m_{11}^{Std}}{m_{10}^{Std}}. \quad (25)$$

The right side of equation (25) is a temperature-dependent constant, which is replaced by the variable φ, to keep the equation readable. Combining equation (25) with equation (18) then results in

$$\frac{m_{10}^{r_n} m_{11}^{r_{n-1}} - m_{10}^{r_{n-1}}(m_B^{r_n} - m_{10}^{r_n})}{m_{10}^{r_n} m_{10}^{r_{n-1}} - (m_{10}^{r_n})^2} = \varphi \quad (26)$$

which is a quadratic equation with $m_{10}^{r_n}$ being the only unknown variable. It can be written in the form

$$(m_{10}^{r_n})^2 + m_{10}^{r_n} \frac{(1-\varphi)m_{10}^{r_{n-1}} + m_{11}^{r_{n-1}}}{\varphi} - \frac{m_{10}^{r_{n-1}} m_B^{r_n}}{\varphi} = 0. \quad (27)$$

The positive solution of quadratic equation (27) for $m_{10}^{r_n}$ results in the mass of ^{10}B in the rock after dehydration step *n*. All other parameters are calculated by using the simple equations (18)–(22).

Evolution of B concentrations in a fluid migrating through filter rock

B concentrations in a fluid migrating from the dehydrating slab towards the site of tourmaline formation within the exhumation channel are modelled. The model is based on mass balance calculations, similar to those used for modelling dehydration.

The following definitions are used: f/r is the fluid/rock mass ratio during each step of interaction, D_B is the partition coefficient of B between rock and fluid, $c_B^{f_n}$ is the concentration of B in the fluid after interaction step *n*, $c_B^{f_{n-1}}$ is the concentration of B in the fluid before interaction step *n*, $c_B^{r_n}$ is the concentration of B in the rock after interaction step *n*, $c_B^{r_{n-1}}$ is the concentration of B in the rock before interaction step *n*, m_{f_n} is the mass of fluid after interaction step *n*, $m_{f_{n-1}}$ is the mass of fluid before interaction step *n*, m_{r_n} is the mass of rock after interaction step *n*, $m_{r_{n-1}}$ is the mass of rock before interaction step *n*, $m_B^{f_n}$ is the mass of B in the fluid after interaction step *n*, $m_B^{f_{n-1}}$ is the mass of B in the fluid before interaction step *n*, $m_B^{r_n}$ is the mass of B in the rock after interaction step *n*, and $m_B^{r_{n-1}}$ is the mass of B in the rock before interaction step *n*.

No hydration or dehydration of the rock is suggested, and, therefore, the masses of fluid and rock are constant:

$$m_{r_{n-1}} = m_{r_n} \quad (28)$$

and

$$m_{f_{n-1}} = m_{f_n}. \quad (29)$$

The fluid/rock ratio (f/r) is the mass ratio of fluid to rock:

$$f/r = \frac{m_f}{m_r}. \quad (30)$$

Mass balance of B in fluid and rock before and after interaction is given by

$$m_B^{r_{n-1}} + m_B^{f_{n-1}} = m_B^{r_n} + m_B^{f_n}. \quad (31)$$

The partition coefficient D_B is defined as the concentration ratio of B in fluid and rock after interaction:

$$D_B = \frac{c_B^{f_n}}{c_B^{r_n}}. \quad (32)$$

The concentration of B is defined by the mass of B divided by the mass of rock or fluid, respectively:

$$c_B^{r_n} = \frac{m_B^{r_n}}{m_{r_n}} \quad (33)$$

and

$$c_B^{f_n} = \frac{m_B^{f_n}}{m_{f_n}}. \quad (34)$$

Combining equations (32), (33) and (34) results in

$$D_B = \frac{m_B^{f_n} \cdot m_{r_n}}{m_B^{r_n} \cdot m_{f_n}}. \quad (35)$$

or

$$m_B^{r_n} = \frac{m_B^{f_n}}{D_B(m_{f_n}/m_{r_n})}. \quad (36)$$

Combining equations (30), (31) and (36) results in

$$m_B^{r_{n-1}} + m_B^{f_{n-1}} = m_B^{f_n} + \frac{m_B^{f_n}}{D_B(f/r)}. \quad (37)$$

This equation can be solved for the mass of B in the fluid after interaction:

$$m_B^{f_n} = \frac{m_B^{r_{n-1}} + m_B^{f_{n-1}}}{D_B(f/r) + 1}. \quad (38)$$

Concentrations of B in fluid and rock after interaction can be calculated by using equations (33) and (34), after calculating the masses of B in fluid and rock using equations (38) and (35).

Evolution of B isotope ratios in a fluid migrating through filter rock

Boron isotope ratios were calculated based on equation (27). However, the mass balance used in this equation has to take in account the amount of ^{10}B and ^{11}B contributed by the fluid before interaction with the rock. Therefore, $m_{10}^{r_{n-1}}$ was replaced by $(m_{10}^{r_{n-1}} + m_{10}^{f_{n-1}})$ and $m_{11}^{r_{n-1}}$ by $(m_{11}^{r_{n-1}} + m_{11}^{f_{n-1}})$, resulting in

$$(m_{10}^{r_n})^2 + m_{10}^{r_n}\frac{(1-\varphi)(m_{10}^{r_{n-1}} + m_{10}^{f_{n-1}}) + (m_{11}^{r_{n-1}} + m_{11}^{f_{n-1}})}{\varphi} - \frac{(m_{10}^{r_{n-1}} + m_{10}^{f_{n-1}})m_B^{r_n}}{\varphi} = 0 \quad (39)$$

The positive solution of quadratic equation (39) for $m_{10}^{r_n}$ results in the mass of ^{10}B in the rock after interaction step n. All other parameters are calculated by using the simple equations (17), (18) and (22), and the expansions of equations (19) and (20) displayed below.

Equation (19) is expanded to

$$m_{10}^{r_n} + m_{10}^{f_n} = m_{10}^{r_{n-1}} + m_{10}^{f_{n-1}} \quad (40)$$

and equation (20) is expanded to

$$m_{11}^{r_n} + m_{11}^{f_n} = m_{11}^{r_{n-1}} + m_{11}^{f_{n-1}}. \quad (41)$$